Applied Energy 400 (2025) 126528

Contents lists available at ScienceDirect

Applied Energy

journal homepage: www.elsevier.com/locate/apenergy

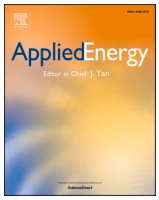

Multi-method optimization of solar district energy systems with battery and thermal energy storage via real-time TRNSYS-Python coupling

Ruslan Kotegov [a], Mohamed Abokersh [b], Carles Mateu [c], Adedamola Shobo [a], Dieter Boer [a], Manel Vallès [a,*]

[a] University of Rovira i Virgili, Department of Mechanical Engineering, Av. Paisos Catalans 26, 43007 Tarragona, Spain
[b] Logitech, Cork, Ireland
[c] University of Lleida, GREiA Research Group, 25001 Lleida, Spain

HIGHLIGHTS

- A hybrid multi-method approach optimizes Solar District Energy Systems (SDES).
- The framework balances cost, environmental impact, and market adaptability.
- SDES achieves over 90 % solar fraction, minimizing fossil fuel reliance.
- Economically viable SDES reduces operating costs by 66.7 %.
- Grid export policies strongly influence system sizing and feasibility.

ARTICLE INFO

Keywords:
Solar district energy systems (SDES)
Life-cycle assessment
Techno-economic analysis
Multi-objective optimization
Renewable energy systems
TRNSYS-Python coupling

ABSTRACT

Transitioning to sustainable energy is vital for decarbonizing energy systems. Solar District Energy Systems (SDES) offer a viable alternative to fossil fuels, but face challenges related to cost, intermittency, and optimization. This study proposes a high-fidelity, fully automated optimization framework for SDES that integrates TRNSYS simulations with a dynamic Python-based controller to jointly minimize life cycle cost and environmental impact. The core innovation lies in the seamless, real-time coupling of simulation and optimization using a hybrid multi-method strategy – combining metaheuristic, heuristic, and stochastic algorithms – without reliance on surrogate models or manual intervention. A Feature Importance Scoring (FIS) module adaptively prioritizes influential variables, enabling efficient convergence and reduced computational cost. The framework is applied to a real Mediterranean case study, assessing PV, battery, and thermal storage integration under economic and environmental criteria. Results show that the proposed SDES achieves a solar fraction above 90 %, ensuring long-term sustainability with minimal fossil fuel reliance. The most cost-effective solution cuts operating costs by 66.7 %, reaching €70.8 million over the system's lifetime, while the environmentally optimal configuration lowers the baseline environmental impact by 29.8 %. Sensitivity analysis reveals that electricity prices strongly influence cost and system sizing, whereas natural gas prices have minimal effect. Overall, the

Abbreviations: ANN, Artificial Neural Network; AUX, Auxiliary heater; BESS, Battery Energy Storage Systems; CEPCI, Chemical Engineering Plant Cost Index; CL, Change logic; COL, Solar collector field; CST, Change Significance Threshold; CV, Cross-validation; DDDM, Data-driven decision-making; DHC, District Heating and Cooling; DHW, Domestic hot water; DHWT, Domestic hot water tank; DP, Dynamic Programming; ECOT, Estimated Continuous Operation Time; EP, Electricity production; FG, Foam glass gravel; FIS, Feature Importance Scoring; FRW, Focused Random Walks; FSOC, Fractional state of charge; GA, Generic Algorithm; GASP, Gaussian Sampling Around Point; GBR, Gradient Boosting Regression; GPR, Gaussian Process Regression; HBT, Heating Base Temperature; HP, Heat pump; HPC, High-performance concrete; IGD, Initial data generation; IRENA, International Renewable Energy Agency; KS, Kolmogorov-Smirnov goodness-of-fit test; LCA, Life Cycle Assessment; LCC, Life Cycle Costing; LFP, Lithium iron phosphate battery; LHS, Latin Hypercube Sampling; MILP, Mixed-Integer Linear Programming; MTBF, Mean Time Between Failures; MW, Mineral wool; NC, Normal concrete; NPC, Net Present Cost; PSO, Particle Swarm Optimization; PV, photovoltaic panel; PVGIS, Photovoltaic Geographic Information System; RF, Refinement found; SDES, Solar District Energy Systems; SDH, Solar District Heating; SEC, Specific economic cost; SH, Space heating; SOC, State of charge; SST, Seasonal storage tank; STC, Solar thermal collector; TES, Thermal Energy Storage; TOPSIS, Technique for Order of Preference by Similarity to the Ideal Solution; TRNSYS, Transient System Simulation Tool; UHPC, Ultra-high-performance concrete; XPS, Extruded polystyrene.

* Corresponding author.
E-mail address: manel.valles@urv.cat (M. Vallès).

https://doi.org/10.1016/j.apenergy.2025.126528
Received 28 April 2025; Received in revised form 3 July 2025; Accepted 23 July 2025
Available online 6 August 2025

method yields significant improvements over traditional deterministic or surrogate-based approaches, demonstrating its potential to support scalable, cost-effective energy planning in low-carbon urban districts.

1. Introduction

Since the 1970s, the global energy sector has undergone a profound transformation driven by technological advancements, policy interventions, and market evolution. The 1973 oil crisis acted as a catalyst for energy diversification, prompting extensive research into renewable energy sources, particularly solar and wind power [1]. Over the following decades, improvements in photovoltaic (PV) technology, thermal energy storage (TES), and district heating (DH) systems enabled the integration of solar-driven energy solutions into urban energy networks. By the late 1980s, silicon-based PV cells had surpassed 15 % efficiency under laboratory conditions [2], while countries like Denmark pioneered large-scale solar district heating (SDH) projects to maximize thermal efficiency and reduce dependence on fossil fuels [3].

The increasing urgency of climate change mitigation and energy security concerns led to significant policy measures, including the Kyoto Protocol in 1997, which set binding emission reduction targets for industrialized nations [4]. By the 2000s, rapid advancements in lithium-ion battery technology and thermal storage further facilitated the integration of solar energy into district networks [5]. Today, with the European Union's Green Deal targeting a 55 % reduction in greenhouse gas emissions by 2030, Solar District Energy Systems (SDES) are emerging as a key solution in the transition toward carbon-neutral energy infrastructures [6,7].

SDES integrates multiple energy technologies, including solar thermal collectors, PV systems, heat pumps, and storage solutions, to provide heating, cooling, and electricity to urban districts [8]. Unlike conventional district heating networks that rely on cogeneration plants or biomass boilers, SDES primarily harness solar energy, reducing fossil fuel dependency and enhancing energy self-sufficiency [9]. A crucial advantage of these systems is their ability to couple multiple energy sectors, allowing simultaneous utilization of solar energy for various end-uses. Large-scale seasonal thermal storage solutions have demonstrated remarkable solar fractions, exceeding 90 % in long-term operation. Notable examples include the Drake Landing Solar Community in Canada, which achieved a 97 % solar fraction in its fifth year of operation [10], and several European projects that have successfully integrated seasonal heat storage to optimize solar utilization. Additionally, combining PV generation with battery storage has improved self-consumption rates, reducing reliance on grid electricity and mitigating the impact of declining feed-in tariffs [11].

Despite these promising advantages, SDES still faces critical challenges in its design and operation. The intermittency of solar energy necessitates advanced storage strategies, including stratified TES and battery energy storage systems (BESS), to ensure continuous operation and peak load management [12]. Furthermore, the integration of multiple energy sources introduces complex thermodynamic interactions, requiring sophisticated optimization techniques to achieve efficient system operation. Conventional rule-based control strategies often fail to account for nonlinear thermal dynamics, leading to suboptimal performance [13]. Economic viability also remains a key concern, as SDES projects must balance investment costs with long-term environmental benefits. While decreasing PV and battery costs have improved financial feasibility, thermal storage solutions continue to be cost-sensitive, requiring detailed life-cycle assessments to evaluate long-term profitability [14].

In recent years, the optimization of SDES has become a growing research focus, with particular emphasis on economic feasibility, environmental impact reduction, and operational efficiency. Historically, district heating and cooling (DHC) networks were optimized using deterministic approaches such as Mixed-Integer Linear Programming (MILP) and Dynamic Programming (DP), primarily applied to conventional fossil-fuel-based systems [15]. As renewable energy sources, particularly solar thermal and PV, have been integrated into district networks, the complexity of optimization has increased, necessitating more advanced computational techniques [16]. Several methodologies have been explored, including metaheuristic algorithms such as Genetic Algorithms (GA) and Particle Swarm Optimization (PSO), as well as surrogate-based optimization methods that leverage Artificial Neural Networks (ANN) or Gaussian Process Regression (GPR) to approximate system performance and reduce computational time [17,18].

However, existing optimization strategies present several limitations. Many studies rely on a single optimization technique, which can restrict solution diversity and increase the risk of convergence to local optima [19]. Deterministic methods, while effective for small-scale applications, become computationally intractable for large-scale SDES networks due to the high dimensionality of the optimization space [20,21]. Additionally, surrogate-based models often require frequent retraining when input parameters change, limiting their real-time adaptability and leading to extrapolation errors when applied beyond their training datasets [22]. Another limitation is the static nature of traditional sensitivity analysis methods, which rank design variables based on predefined conditions rather than dynamically adjusting them during the optimization process [22,23]. Furthermore, most SDES optimization studies rely on separate simulation and optimization steps, which prevents continuous system adaptation based on real-time feedback. The lack of direct coupling between simulation platforms such as TRNSYS (Transient System Simulation Tool) and optimization frameworks leads to inefficiencies in result validation and decision-making [24].

To address these challenges, this study aims to develop an advanced hybrid multi-method optimization framework for SDES, integrating multiple search strategies to enhance computational efficiency, adaptability, and fully automated decision-making. The proposed approach incorporates metaheuristic exploration [25,26], stratified sampling techniques [27,28], heuristic refinement [29–31], and stochastic search methods to improve optimization robustness [32]. Additionally, a dynamic Feature Importance Scoring (FIS) mechanism based on Gradient Boosting Regression (GBR) is introduced to prioritize influential design variables during the optimization process, reducing computational costs and enhancing interpretability. Several articles explore TRNSYS-Python integration, but they are not comprehensive enough in terms of seamless TRNSYS-Python integration (still requires human intervention to finalize decisions) or don't mention Python or any other tool used for automatic data processing [33–37]. A fully integrated TRNSYS-Python optimization workflow that enables on-the-fly system reconfiguration without retraining delays has yet to be developed.

Previous studies have used methods such as MILP, surrogate-based optimization, and single-method metaheuristics (e.g., PSO, GA) for planning and operation of renewable energy systems. However, these approaches often suffer from well-documented limitations, such as inflexibility to changing parameters, lack of real-time simulation coupling, or single-point exploration strategies. In contrast, our proposed framework integrates real-time TRNSYS–Python simulation with multiple search algorithms and adaptive feature importance scoring, enhancing both adaptability and robustness. Table 1 provides a conceptual comparison highlighting the limitations of conventional approaches and how the present work addresses them.

The novelty of this study lies in the development of a fully automated, real-time optimization framework that seamlessly couples TRNSYS simulations with multiple search strategies (such as metaheuristic, heuristic, stochastic, and statistical) via Python integration,

Table 1
Strengths and limitations of real-time simulation-based vs. conventional optimization methods.

Feature	TRNSYS–Python Integration	Traditional Optimization Methods* [38]
Flexibility	Offers broad adaptability through extensive Python libraries, enabling tailor-made workflows.	Restricts users to a fixed set of algorithms with no dynamic runtime flexibility for strategy changes.
Data Handling	Enables efficient processing of large and complex datasets through advanced data tools.	Lacks built-in mechanisms for internal or post-simulation data handling—must be managed externally.
Machine Learning Compatibility	Easily incorporates ML models for predictive analytics and adaptive optimization.	No native support for machine learning or adaptive modeling methods.
Computational Efficiency	Uses heuristic and adaptive sampling to avoid redundancy, accelerating convergence.	While individual GenOpt algorithms may be adaptive, the lack of runtime switching can hinder performance.
Optimization Versatility	Supports a hybrid of methods for global exploration and local refinement.	Only one optimization method per run is allowed, without support for dynamic switching.
Customization & Transparency	Fully scriptable with open-source control, offering deep customization.	Limited to basic XML configurations, restricting advanced customization.
Diagnostics and Debugging	Includes robust logging and error reporting tools for detailed diagnostics.	Minimal built-in diagnostics; users must build external tools for tracking and debugging.
Feature	*Advantages of TRNSYS–Python Framework*	*Surrogate-based Limitations [39,40]*
Accuracy of Results	Executes full TRNSYS simulations for precise, high-fidelity outputs.	Relies on approximations, which can misrepresent behavior outside the training range.
Data Requirements	Performs well with smaller datasets, reducing data collection burden.	Requires large pre-collected datasets for training before use.
Adaptability to Model Updates	Accommodates changes to model structure or parameters in real-time without retraining.	Needs complete retraining whenever the underlying model is significantly altered.

* Includes single-algorithm metaheuristics, deterministic formulations, and GenOpt-based tools.

eliminating the need for manual intervention or model retraining during the optimization process. Unlike existing methods, which either rely on static surrogate models or decoupled simulation-optimization steps, this framework dynamically adapts to system responses using an FIS mechanism and enables on-the-fly system reconfiguration. This scientific contribution advances the field by delivering a high-fidelity, scalable optimization approach that captures complex thermodynamic interactions within SDES while significantly improving computational efficiency and decision-making accuracy.

2. Methodology

In order to accomplish the stated objectives, a multi-objective optimization of the SDES was conducted using predictive modeling. This optimization targeted a reduction in both the system's cost and environmental impact. Concurrently, a comprehensive assessment of the system's performance was undertaken to ensure its effective fulfillment of the energy requirements of a residential community.

The foundation of our methodology is energy modeling, a cornerstone in renewable energy system optimization, crucial for analyzing and refining energy processes. The implementation of this methodology was facilitated by the TRNSYS [41], a software that is seamlessly integrated with Python. To facilitate the transfer of all necessary variables to TRNSYS for simulation purposes, we leveraged the "subprocess" Python library [42]. This integrated approach enabled the exploration of diverse system configurations, overcoming geographical limitations and accommodating a wide range of system characteristics, ultimately delivering robust solutions for renewable energy systems.

Data preparation for optimization in terms of economic and environmental analysis is presented in the Annex (A-1).

2.1. Optimization framework

The primary objective of the optimization procedure is to concurrently minimize the total SDES cost and its environmental footprint (objective functions) while maintaining compliance with the technical requirements. The proposed algorithm for the sustainable assessment of a system is outlined in Fig. 1.

The present section delineates the sequential steps of an efficient optimization framework designed to ascertain the optimal configuration for sustainable energy systems. The methodology leverages data-driven decision-making (DDDM) to hone in on the most influential variables using FIS and k-fold cross-validation (CV) within a machine-learning context. For the proposed SDES system, the objective function is to optimize the NPC, and the RCP is given as follows:

$$
\begin{aligned}
&min \\
&s.t.\{f_1(x), f_2(x)\} \\
&h_i(x) = 0, \\
&g_j(x) \geq 0, \\
&\forall i \in \{1, \ldots, m\} \\
&\forall j \in \{1, \ldots, p\} \\
&lb_q \leq x_q \leq ub_q \forall q \in \{1, \ldots, n\}
\end{aligned} \tag{1}
$$

Where x is the vector of design variables, f_1 is RCP and f_2 is NPC $h_i(x)$; $h_i(x)$ and $g_j(x)$ are the equality and inequality constraints respectively that must be simultaneously satisfied. The equality constraints correspond to the physics of physical systems solved in TRNSYS (e.g. energy balances) and inequality constraints correspond to the technical evaluation of SDES. lb_q and ub_q are the lower and upper bounds, respectively, foTr each variable x_q; m, p, and n are the total number of equality and inequality constraints, and the total number of design variables constraints respectively. Through these constraints, annual solar efficiency is maintained $> 60\%$, and renewable energy fraction for thermal energy is maintained $> 50\%$ as recommended by Bauer et al. [43] and Tecnalia [44].

2.2. Initial data generation (IGD): building a strong optimization foundation

The optimization process starts with the creation of an initial dataset using Latin Hypercube Sampling (LHS). This method ensures a uniform distribution across key design variables such as STC and PV areas, Li-ion battery, SST, and DHWT volumes. The dataset is validated using the Kolmogorov-Smirnov (KS) test [45], which compares the LHS sample distribution to the full dataset, ensuring it accurately represents the system's design space. This ensures the initial dataset provides a reliable foundation for optimization by identifying promising design areas.

2.2.1. Identifying key influencing variables

To reduce the computational burden and improve convergence efficiency, the Data-Driven Decision-Making (DDDM) module guides the optimization process by identifying the most influential variables using FIS within a machine-learning framework. FIS assigns scores to input variables based on their impact on objectives, enabling the focus on

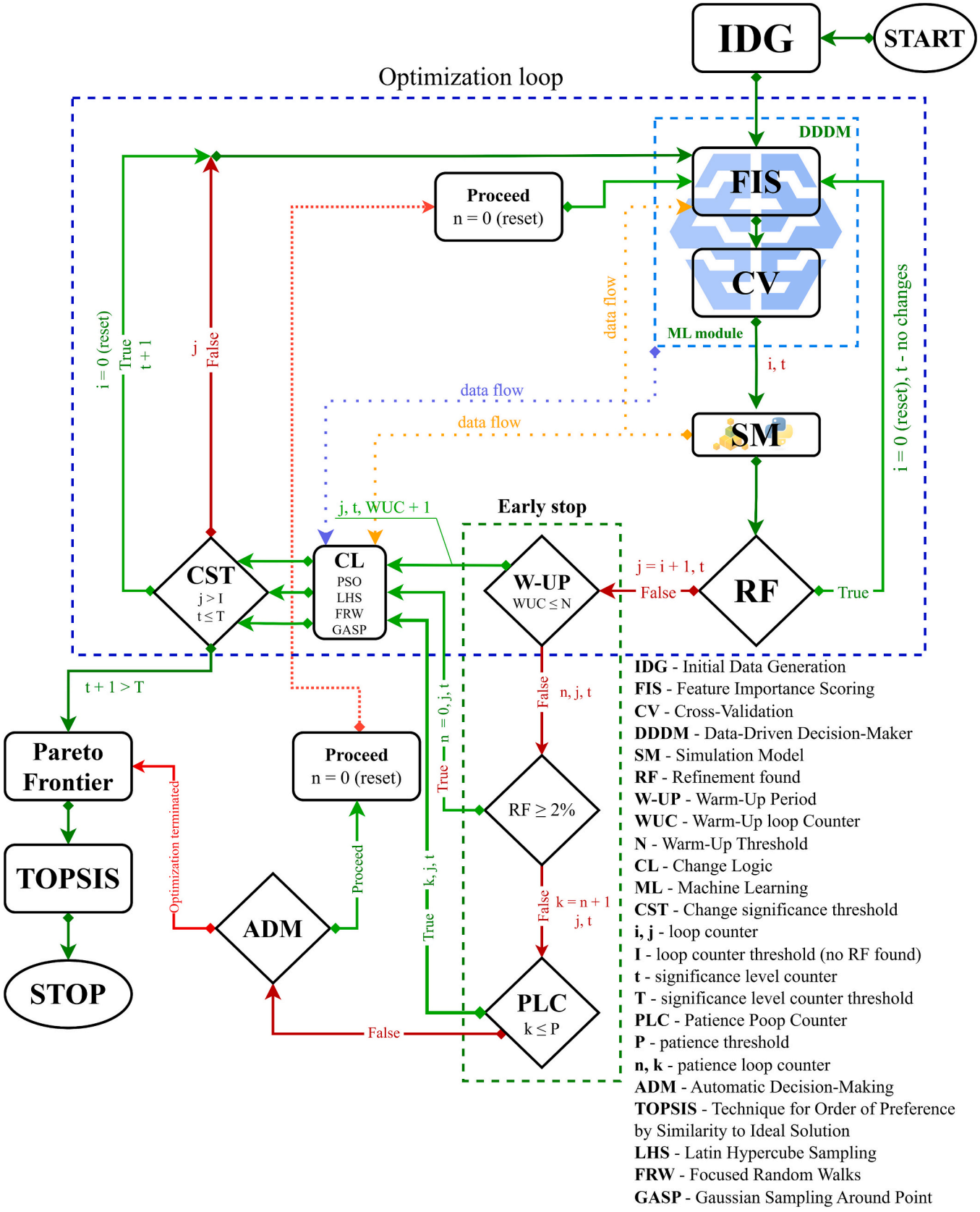

Fig. 1. Optimization framework.

high-priority areas.

This strategy enables a selective focus during optimization: highly influential variables are prioritized for exploration, while less impactful ones are either fixed or varied within narrower ranges. This approach allows the framework to dynamically adapt to the evolving sensitivity of the system and reduces the number of unnecessary simulations, particularly in the later stages when the search space is refined. By integrating k-fold cross-validation (CV), the module minimizes overfitting and ensures model robustness. This data-driven approach efficiently narrows the search space and accelerates convergence.

2.2.2. Simulation model

The Simulation Model is a module that acts as the execution bridge between the Python-based optimization routine and the TRNSYS simulation environment. It handles the preparation of input files, runs deterministic energy performance simulations in TRNSYS, and collects structured outputs for evaluation. The Simulation Model also manages preprocessing (e.g., organizing runs) and postprocessing (e.g., consolidating results for refinement and decision-making). Since TRNSYS produces consistent outputs without stochastic variation, each design configuration is simulated only once, eliminating the need for repeated runs or uncertainty quantification such as error bars or confidence intervals.

2.2.3. Refinement found (RF) and early stop: ensuring efficient iterations

To avoid redundant evaluations and excessive computation time, the optimization framework integrates two key mechanisms: Refinement Found (RF) and Early Stop.

In each iteration of the optimization loop, the RF module processes data. This data is evaluated to detect any significant enhancements or adjustments compared to the previous iteration regarding the objective functions. If an improvement is detected (RF is true), there is no need to alter the logic, and with the continuous data input from the SM, the same approach is utilized in the DDDM module. Conversely, if no improvement is detected (RF is false), the Early Stop module is activated to verify if the stopping conditions are met.

2.2.4. Adaptive strategies for solution exploration

The Change Logic (CL) module applies advanced sampling techniques to explore the solution space effectively. These techniques are listed in Table 2:

The choice of method depends on feedback from the system model and optimization history, ensuring adaptive and efficient exploration.

2.2.5. Prioritizing meaningful adjustments

The Change Significance Threshold (CST) module evaluates whether changes in variables are significant enough to impact the optimization objectives. It dynamically adjusts the threshold for changes based on system feedback, balancing precision and adaptability. This mechanism ensures that the optimization remains focused on meaningful adjustments.

Table 2
Sampling strategies applied in optimization.

Technique	Sampling type	Description	Reference
Latin Hypercube Sampling (LHS)	stratified	Ensures uniform exploration across variables	[27,28]
Focused Random Walks (FRW)	heuristic	Generates samples around promising solutions to refine them	[29–31]
Gaussian Sampling Around Point (GASP)	stochastic	Introduces controlled randomness near optimal points for better exploration	[32]
Particle Swarm Optimization (PSO)	metaheuristic	Simulates collaborative behavior to avoid local optima and find a global solution	[25,26]

2.2.6. Guiding the optimization process

The optimization loop iteratively refines solutions by generating new data, assessing improvements, and recalibrating focus. The process continues until predefined stopping conditions, such as achieving convergence in objective functions or reaching a maximum iteration count, are met. Each loop iteration improves the feature importance rankings and predictions, moving closer to the optimal configuration.

2.2.7. Balancing trade-offs in multi-objective optimization

Anchor points, representing extreme solutions (e.g., minimum cost or environmental impact), are refined to ensure accuracy. Using the Non-Dominated Sorting Genetic Algorithm II (NSGA-II), a Pareto-based evolutionary search is conducted where non-dominated solutions are identified, forming a Pareto frontier that balances trade-offs between multiple objectives. The Technique for Order of Preference by Similarity to the Ideal Solution (TOPSIS) [46] ranks these solutions, incorporating variable weights to highlight the optimal trade-off design that balances environmental and economic goals.

2.2.8. Highlighting optimal solutions

The final optimization results are visualized through the Pareto frontier, which displays trade-offs between cost and environmental impact. Convergence indicates that the framework has successfully identified optimal solutions. This step provides a clear overview of the most sustainable and cost-effective system designs, aiding in decision-making and implementation.

The proposed optimization approach is built on a tightly integrated TRNSYS-Python framework, where both environments play distinct yet complementary roles. Python acts as the central controller, managing the full optimization workflow – from generating initial design samples to adaptively selecting and switching among statistical, heuristic, stochastic, and metaheuristic search strategies. It also handles decision-making, feedback interpretation, and refinement processes. TRNSYS functions as the high-fidelity simulation core, tasked with accurately evaluating the energy performance of each system configuration. At every iteration, Python creates the necessary input files, launches TRNSYS simulations via automated scripts, and processes the resulting outputs. These simulation results are used to update internal performance indicators, inform the next set of decisions, and assess convergence status. This modular and dynamic coupling avoids reliance on surrogate models, supports real-time system adaptability, and enables scalable exploration of complex, multi-objective energy system design spaces.

It is important to highlight that the adaptability of the proposed methodology enables the application of diverse algorithms to both the CL and DDDM modules, allowing the model to be tailored to the specific demands of each optimization problem.

The exhaustive list of libraries used in optimization is presented in the SI (Table 1).

3. Case study

3.1. Climate and demand profiles

For the implementation of the proposed SDES concept, a small settlement called Falset (41°08′46″N 0°49′12″E) in the autonomous community of Catalonia, Spain, has been selected. This community comprises 1712 dwellings, spread across 1058 buildings [47]. The SDES is designed to meet the 24-h demands for space heating, hot water, and electricity. The heating system operates at a water temperature of 50 °C, while the hot water system operates at 60 °C [48].

Data from the cadastral register regarding the various types of

building clusters in the locality were utilized to calculate the heating load [49]. The thermal load for every 100 square meters of each cluster is based on the "Segmentation of the Residential Housing Stock in Spain into Typological Clusters" [50]. The hourly heating load is determined using information from the "Energy Statistics - Cooling and Heating Degree Days", which relies on a Heating Base Temperature (HBT) of 18 °C during the heating season of a typical year, spanning from October to May [51]. The meteorological data used is specific to the selected location of Falset and was obtained from the PVGIS (Photovoltaic Geographic Information System) platform [52].

The hourly fractional load for the residential hot water system was calculated using the methodology detailed in the "Basic Document HE Energy Saving", which is part of the "Technical Building Code." This is reflected in Table 3. The daily and hourly water temperature was determined according to the method described by Żukowski M [53].

The daily domestic hot water demand $Q_{DHW}(J)$ for the municipality was defined as:

$$Q_{DHW} = Pop \bullet V \bullet \rho \bullet C \bullet \left(T_{sup} - T_w\right), \quad (2)$$

where:

Pop – population per municipality (number of people).

V – the domestic hot water (DHW) volume per person per day, 0.030 m^3 [54].

ρ – water density, kg/m^3.

C – specific water heat capacity, J/kg ^oC.

T_{sup} – hot water supply temperature, ^oC [55].

T_w – tap water temperature, ^oC.

The typical residential electricity load is derived from data provided for 2019 by the Datadis platform [57]. The total heating, hot water, and electricity loads are 12,087 MWh, 1602 MWh, and 4221 MWh, respectively. Monthly and annual data for these loads, based on hourly measurements, are illustrated in Fig. 2.

3.2. SDES specification and operation

TRNSYS 18 was utilized to analyze and simulate the system's behavior thoroughly. Its capability to model transient systems, combined with its flexibility and user-friendly graphical interface, allowed for an accurate representation of the system's dynamic characteristics and the realistic simulation of the SDES. The computer simulation spanned three consecutive years to ensure the system reached a steady state. The results were projected over the expected lifespan of the system, estimated to be 40 years, with the assumption that weather conditions and load profiles would remain constant throughout this period. The validation of the SDES model was based on the works of Abokersh et al. [58], Tulus et al. [59], and the original concept by Guadalfajara et al. [60]. The primary SDES scheme is illustrated in Fig. 3.

3.2.1. Main SDES components and control strategies

The SDES configuration integrates various components to meet daily requirements for space heating (SH), domestic hot water (DHW), and electricity. The system includes roof-mounted solar thermal collectors (STCs), heat pump (HP), photovoltaic (PV) panels, Li-ion batteries, a stratified storage tank (SST), a domestic hot water tank (DHWT), a central water-to-water heat pump, and auxiliary heaters (AUXs) powered by natural gas.

Electricity needs are addressed through a combination of on-grid PV panels, batteries for energy storage and dispatch, and grid electricity to cover power shortages and support neighborhood electric demand.

During winter, when heating needs peak, the SST operates at a low temperature of 50 °C for space heating, while the DHWT ensures that hot water is available at a higher temperature of 60 °C. Solar thermal collectors primarily supply heat for both SH and DHW demands. However, when their contribution – along with that from the heat pump and SST – is insufficient, the AUXs provide additional heat. The heat generated by the heat pump can flexibly be used for either space heating or DHW needs and may also charge the SST, depending on operational priorities. The HP operates based on the temperature-driven control strategy to maximize solar energy utilization while ensuring a continuous heating supply.

Efficient heat distribution is achieved through counterflow heat exchangers equipped with 'Y' valves, which ensure precise control of flow direction based on demand. The STCs, heat pump, and SST work together to optimize heat delivery for both SH and DHW. For space heating, the SST functions as a thermal reservoir, while the DHWT fulfills daily hot water requirements.

The system's electricity supply is carefully balanced. PV panels generate energy, which is stored in Li-ion batteries for later use. These batteries discharge to meet the load when solar generation is unavailable or insufficient. Any unmet electric demand is compensated by drawing power from the grid. This hybrid approach ensures reliable electricity for SDES equipment and the neighborhood, even during periods of low solar availability.

At the core of this system design are advanced TRNSYS model components, including photovoltaic panels (Type 190), Li-ion batteries (Type 549a) pared with the regulator-inverter (Type 48b), solar thermal collectors (Type 1a), a water-to-water heat pump (Type 927), fully stratified storage tanks (Type 4c), counterflow heat exchangers (Type 5b), and auxiliary heaters (Type 6). Together, these components function in synergy to create a resilient and efficient energy solution for both heating and electrical needs.

An effective control strategy is implemented to meet residential heating demands while maximizing the use of solar energy. Four operational modes are established based on the temperature levels of the SDES and are controlled via on/off switches [58].

1) **Mode 1:** In the first mode, the heat from solar collectors is transported to the DHWT with the help of P_1, P_2, and P_5 pumps through HE_2. If solar thermal energy is insufficient for the DHW network, the auxiliary heater (AUX_2) is enabled.
2) **Mode 2:** In the second mode, SH is initiated when a suitable temperature in DHWT (T_{DWT}) is reached, and the temperature of the collector (T_{COL}) is higher than the bottom of SST (T_{SST}). P_1, P_2, and P_3 pumps transfer heat to SST from STC via HE_1.
3) **Mode 3:** In the third mode, both DHW and SH circuits are initiated when the criteria for both operations are met, where $T_{SST} > T_{DHW}$.
4) **Mode 4**: In the fourth mode, HP operates if the solar thermal system cannot meet heating demands. Here $T_{COL} < T_{SST}$, which is less than the reference turn-on temperature of the heat pump (T_{ref}). The heat generated by the HP is used for either SST or DHWT. AUXs meet any uncovered heat demands.

Moreover, the on-grid PV panels combined with Li-ion batteries decrease the amount of electricity purchased from the supply grid, satisfying both the neighborhood's electric demand and the electrical needs of the SDES equipment.

The Li-ion battery and the regulator-inverter are essential components of a photovoltaic system, working together for efficient electricity

Table 3
The hourly fractional DHW demand [56].*

Hour	f_h*	Hour	f_h*	Hour	f_h*	Hour	f_h*
0 h	0.01	6 h	0.03	12 h	0.05	18 h	0.05
1 h	0.00	7 h	0.10	13 h	0.05	19 h	0.07
2 h	0.00	8 h	0.07	14 h	0.04	20 h	0.06
3 h	0.00	9 h	0.07	15 h	0.03	21 h	0.06
4 h	0.00	10 h	0.06	16 h	0.04	22 h	0.05
5 h	0.01	11 h	0.06	17 h	0.04	23 h	0.05

* f_h refers to the fraction concerning the daily total DHW demand.

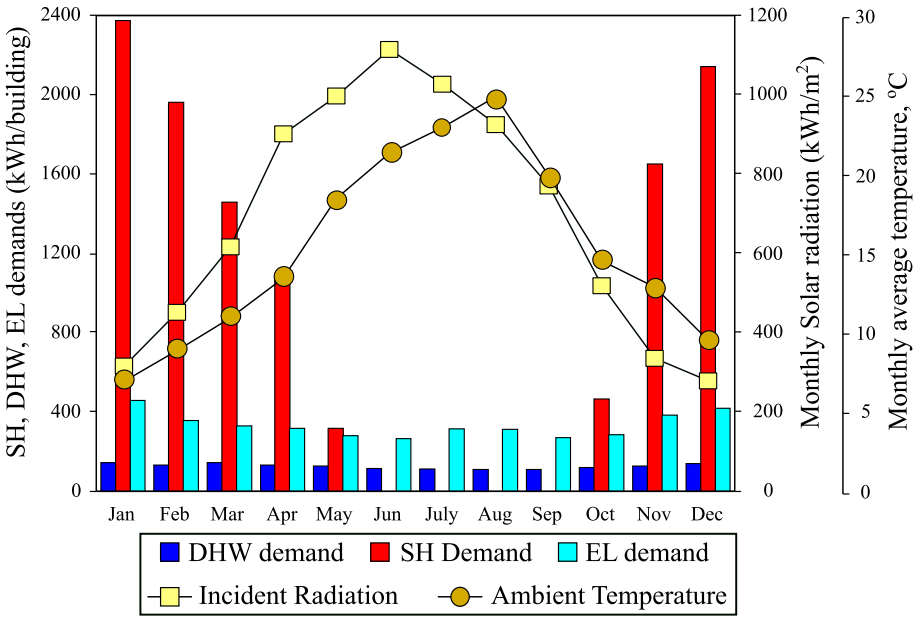

Fig. 2. The monthly climate conditions and the SH, DHW, and Electricity demand profile of the investigated energy community of Falset.

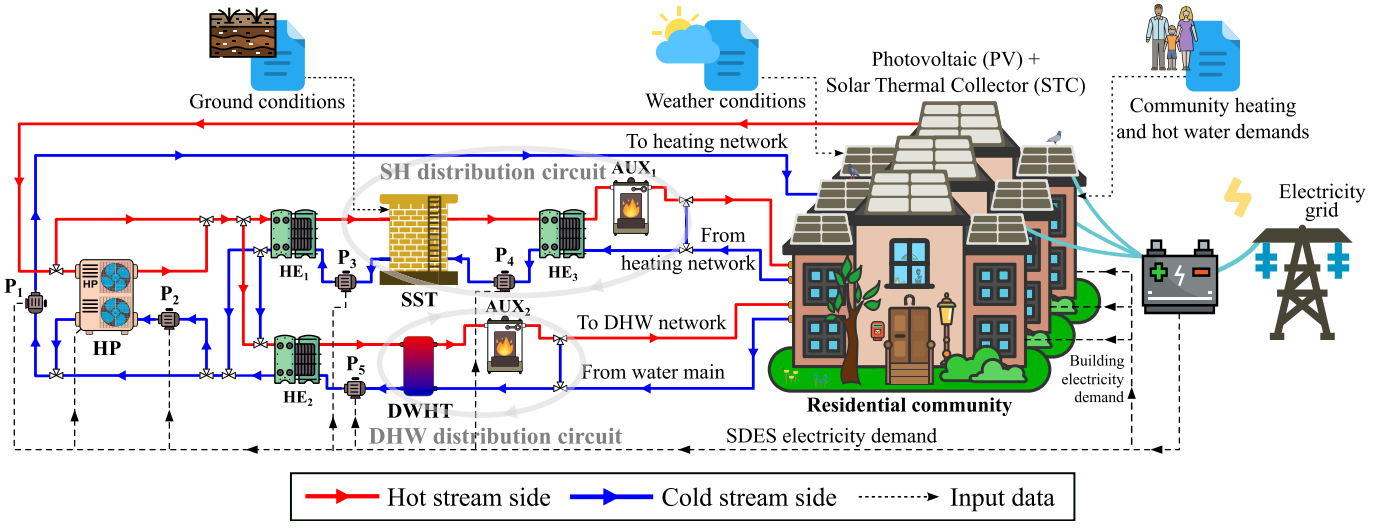

Fig. 3. Solar District Energy System (SDES).

generation, storage, and distribution. The battery manages its state of charge through a voltage model, ensuring optimized energy storage and retrieval. Meanwhile, the regulator channels direct current (DC) from the photovoltaic array to the battery or converts it to alternating current (AC) for use, dynamically balancing energy flows to maintain system efficiency. Supported by a photovoltaic array that captures solar radiation based on local weather data, these components collectively establish an effective framework for sustainable electricity management.

The Type 48b regulator-inverter operates under various regimes based on the battery's state of charge (SOC) and energy demands [61]:

1) **Regime 1:** when the SOC is below a critical threshold, the regulator prioritizes charging the battery by directing all available DC sources, ensuring the battery is sufficiently replenished before supplying power to the load.
2) **Regime 2:** when the SOC is high, exceeding a set limit, the system halts further charging to protect the battery, redirecting excess power to the load or the grid, or preventing the collection of surplus energy from the photovoltaic array.
3) **Regime 3:** when the SOC is between the defined lower and upper limits, the system dynamically balances power flow, charging the battery if excess energy is available and discharging it to meet the load if demand exceeds the array's output.

These operational strategies allow the system to efficiently adapt to varying solar generation and load conditions, ensuring optimal performance and protection for the Li-ion battery while maintaining a consistent power supply.

All information regarding the simulation model, alongside the environmental and economic inputs, is presented in the Annex (A-2).

3.3. *Assumptions and system boundaries*

This study operates under several foundational assumptions to guide the simulation and optimization of the SDES. It is assumed that the

project has a lifespan of 40 years, during which key components such as STCs, PV panels, HP, HEs, DHWT, AUXs, and centrifugal pumps require replacement after 20 years of continuous operation [62]. In contrast, the SST lifetime is set to 80 years [63]. As for the battery, its life cycle is not measured by the duration of continuous operation but by the average number of complete charge/discharge cycles, which range from 2500 to 10,000, according to the literature [64–69]. The average value of 5000 cycles, according to [66] is taken as a reference. The horizon of the dynamic simulation in TRNSYS is 3 years, with the 3rd year being extrapolated to represent the system's performance over the remainder of the project's lifespan. The time resolution for the TRNSYS simulations is set at 1 h. The rooftop area available for solar installations is uniformly distributed across all buildings, with solar thermal collectors prioritized for placement, followed by PV panels. The available rooftop area is calculated following the Saez et al. [70] methodology. Any excess PV panels are installed in nearby fields due to space constraints. This study assumes equipment operation with scheduled replacements and uses long-term averaged meteorological data from PVGIS (2005–2023) [52]. Climate data, derived as a TMY file, is assumed to remain constant throughout the project's duration. The extended database includes decision variables (discrete values) such as the STC area, PV area, battery capacity, SST, and DHWT volumes, which are incremented in standard sizes due to practical construction limitations. The other prime assumptions for the model are outlined in Table 4.

4. Results and discussion

Current work provides sustainable insights into the applicability of the current optimization framework for the economic-environmental optimization of the transient SDES model applied to the real case study. The FIS-based optimization strategy was used to optimize the SDES framework for the residential community of Falset, located in Tarragona province, Spain. The findings provide insights into the system's performance in the current economic landscape, unveil the system's environmental benefits with renewable technologies integrated, and expose the modeling and technical constraints encountered during the simulation process. Owing to the inherent complexity and intricacy of the model, a single simulation cycle ranged from 50 to 70 CPU seconds when run sequentially on a 12th Gen Intel(R) Core(TM) i7-1255U processor with 16 GB of RAM. Python's flexibility enabled the full utilization of computational capabilities, which are limited only by the number of available processor cores. This functionality enabled the concurrent execution of multiple TRNSYS simulations, substantially reducing the optimization time required. It opens up space for experimentation and enhances the accuracy and quality of the results obtained. The results regarding the model's reliability and prediction accuracy are presented in the Annex (A-3).

4.1. Multi-objective optimal solutions

The multi-objective optimization model's capabilities are demonstrated through the Falset case study, which focuses on the design optimization of the SDES in the Mediterranean EU climate zone. Fig. 4 illustrates a set of optimal solutions that define the Pareto frontier resulting from the optimization process.

Table 4
Prime optimization scenario.

Optimization scenario	Thermal Energy Use	Environmental Impact	Allocation*
	All for community use	No negative impact was considered; surplus impact nullified	Not considered

* Allocation: In energy systems, the process of distributing and assessing the impact of produced energy, focusing on the self-consumption share within a community and excluding surplus energy sent to the grid.

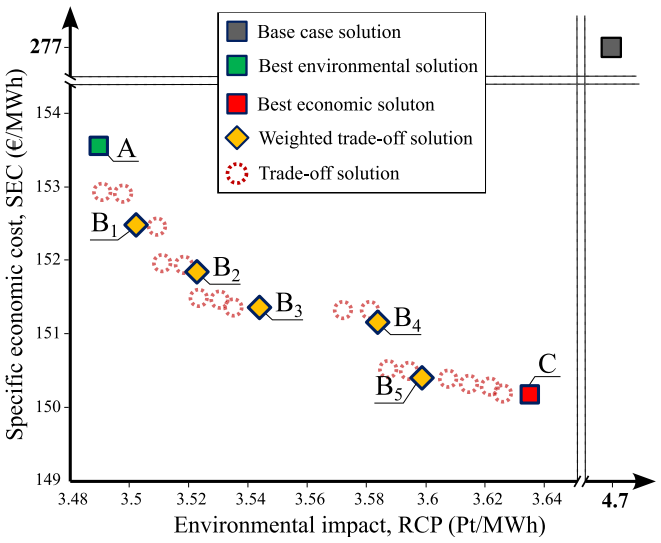

Fig. 4. Pareto set of optimal solutions for the SDES in Falset.
A – min impact solution, C – min cost solution, B_1-B_5 – TOPSIS weighted intermediate/trade-off solutions.

The baseline solution, which does not incorporate any renewable technologies, serves as a benchmark with a specific economic cost (SEC) of 277 €/MWh and an environmental impact (RCP) of 4.7 Pt/MWh. The optimal economically viable solution, referred to as C, achieves a significant cost reduction of 45.8 %, resulting in a price of €150.1 €/MWh compared to the baseline. Meanwhile, the best environmental solution, A, shows a slightly smaller but still impressive price reduction of 44.6 %, bringing its cost to €153.6 €/MWh. In terms of sustainability, solution A demonstrates a decrease of 25.4 % relative to the baseline scenario, resulting in 3.49 Pt/MWh. Solution C, while slightly less effective in this regard, still reduces 22.5 %, bringing its value to 3.64 Pt/MWh. As for the optimal scenarios themselves, the sustainable solution outperforms the cost-efficient option by 4.1 % in environmental performance, while the less expensive option offers a 2.3 % cost savings.

The convergence of optimal solutions corresponds with recent findings from the International Renewable Energy Agency (IRENA) [71] and studies on multi-objective optimization [72]. As renewable energy costs decrease and fossil fuel prices increase, the trade-off between economic and environmental goals diminishes. IRENA (2023) indicates that nearly 86 % of newly commissioned renewable power projects in 2022 were more cost-effective than their fossil fuel-based counterparts, highlighting the shift toward sustainable energy. Furthermore, research on Pareto optimization in energy systems shows that advancements in renewable technologies are reshaping the cost-performance frontier, thereby narrowing the gap between economic and environmental objectives.

4.2. Optimal system designs

The model considered a multitude of decision variables for various system configurations to arrive at the optimal solutions outlined above and illustrated in Fig. 5. The SDES optimal design also became a pivotal consideration for achieving the desired economic and environmental performance. An in-depth analysis of the obtained optimal solutions provided a roadmap for determining the sizing of components in the SDES. There are five primary design decision variables at play: photovoltaic area, solar thermal collector area, seasonal storage tank volume, domestic hot water tank volume, and Li-ion battery capacity. These variables fluctuate and serve as guidelines for the optimal system design, as depicted in Fig. 5. Each diagram features lower and upper whiskers, representing each component's optimization boundaries and a central solid body that indicates the optimal size range for those components.

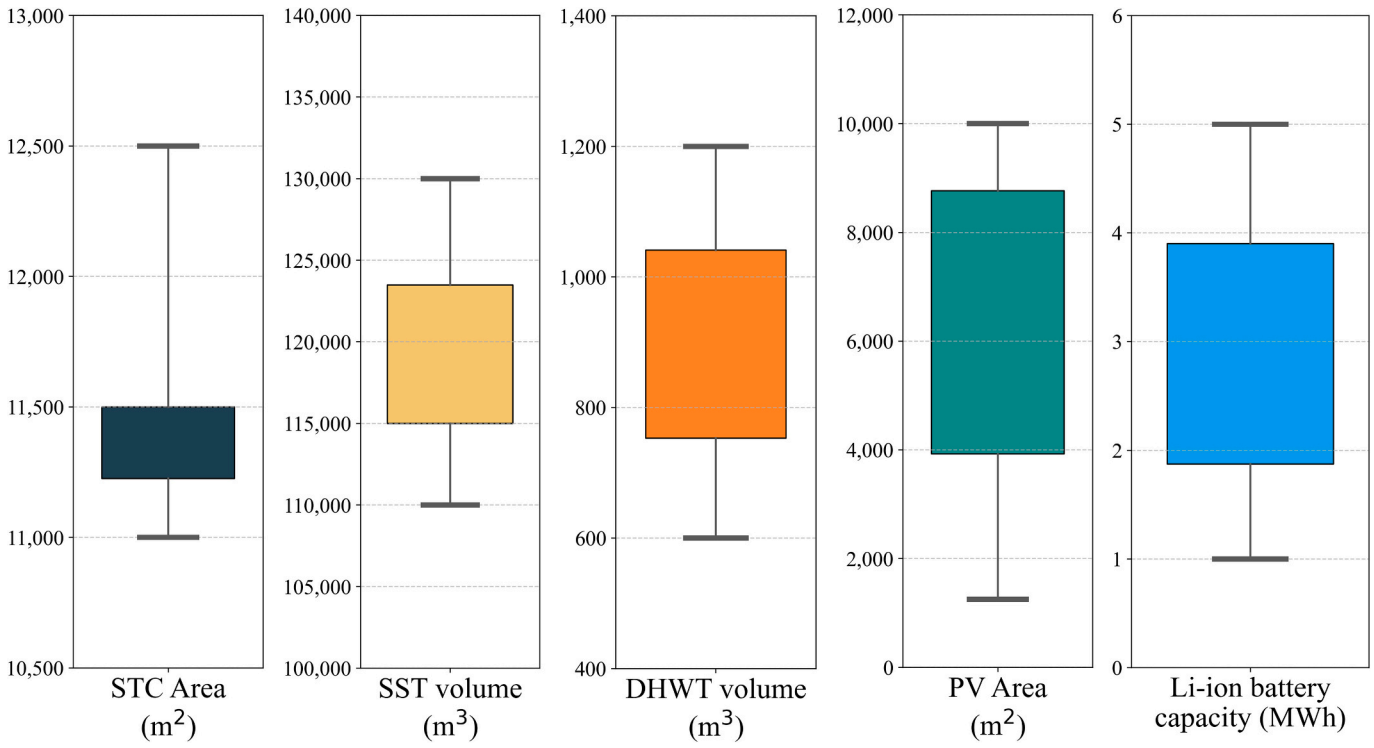

Fig. 5. Guideline for the optimal SDES design.

A detailed size breakdown for each component can be found in the SI (Table 2).

4.3. *Electrical and thermal performance of the system at optimal solutions*

After identifying the optimal system designs through multi-objective optimization, we assessed the system's thermal and electrical performance, the results are provided in Annex A-4. Concerning thermal energy management, Fig. 6 presents a comprehensive analysis of the monthly contributions from various metrics, including solar collectors, stored solar energy, heat pumps, and standalone auxiliary boilers. It is worth noting that the energy stored in the SST is shown with a negative sign, clearly demonstrating the periods of energy accumulation and use.

The active accumulation of energy is most intense between April and October, when solar radiation is at its peak and sufficient not only to meet demand but also to store excess energy for later use. During the cold months from November to March, the phase of active thermal energy consumption occurs. Interestingly, in February and March, the stored energy is not enough to meet heating demands, leading to the use of SH auxiliary heating systems in these months. The absence of the DHW auxiliary heater as well as a heat pump in the diagram implies their insignificant contribution to the energy profile of the system.

For a deeper understanding of system energy management and the counterintuitive behavior of some contributors, it should be considered

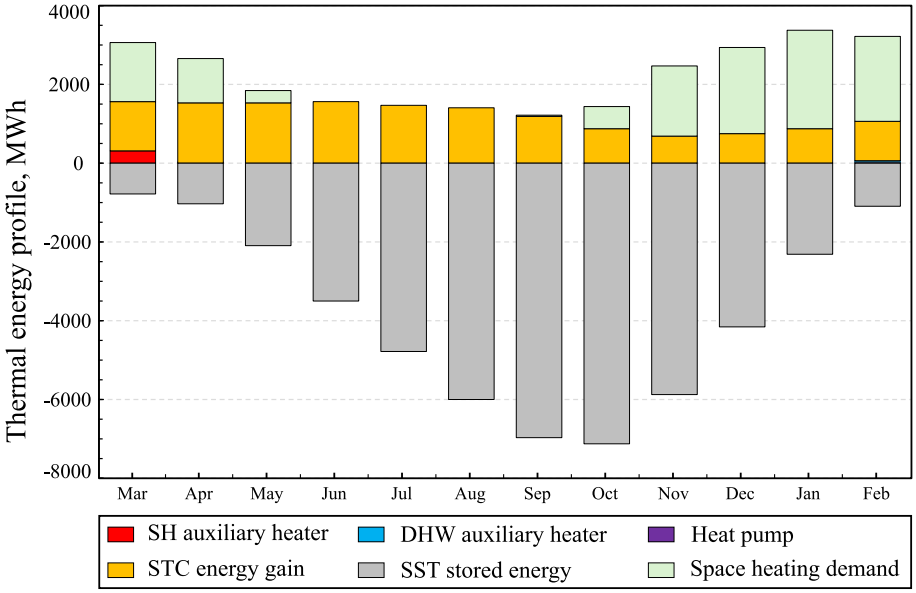

Fig. 6. The annual thermal energy management of the SDES's optimal design.

in context with the solar fraction and the efficiency of individual components. A comparative analysis of solar fraction and efficiency metrics between cost-effective and sustainable solutions is depicted in Fig. 8.

Fig. 7 illustrates the SDES electricity management under two optimal designs (anchor points). The best cost design (Fig. 7a) is marked by increased electricity production and reduced reliance on grid electricity. However, this design also involves a higher discharge of electricity back to the grid. The lower overall cost of this solution stems from decreased dependence on the grid and the ability to monetize excess electricity.

In contrast, the best impact design (see Fig. 7b) involves reduced power generation, leading to increased grid dependency and minimal grid export, which increases the overall cost of purchased power and reduces the potential for monetizing surplus. The reliance on the grid is offset by a smaller PV area, resulting in a lower environmental impact of this solution. The introduction of monetized grid export has reversed the conventional trade-off in energy system optimization: a higher share of renewables now results in lower costs but greater environmental impact, whereas reduced renewable deployment increases costs while lowering overall impact.

The global solar fraction (see Fig. 8) in the context of a cost-effective solution amounts to 91 %, whereas the sustainable solution demonstrates a slightly lower solar fraction at 82.5 %. This disparity is

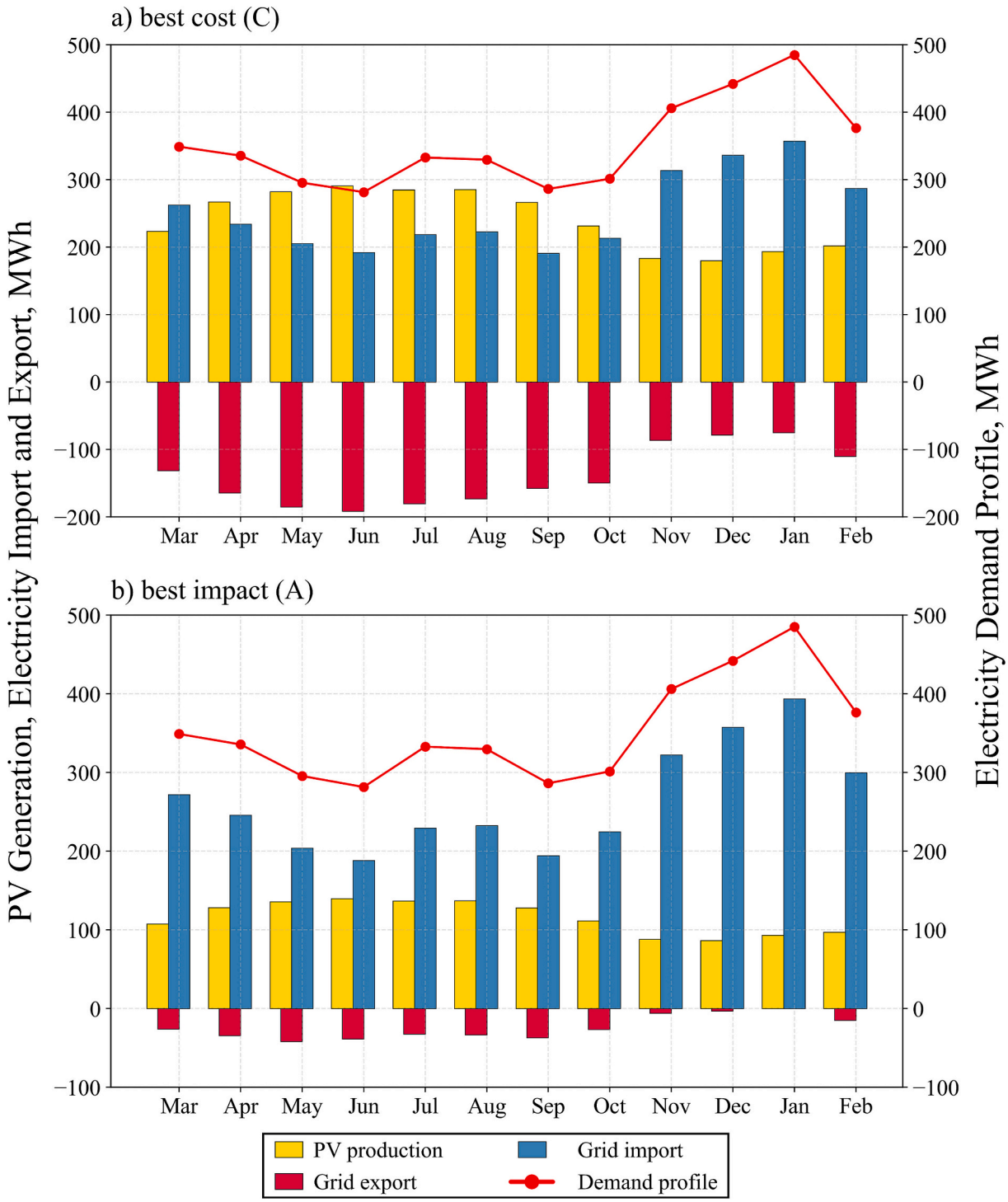

Fig. 7. The annual electrical energy management of the SDES's optimal design.

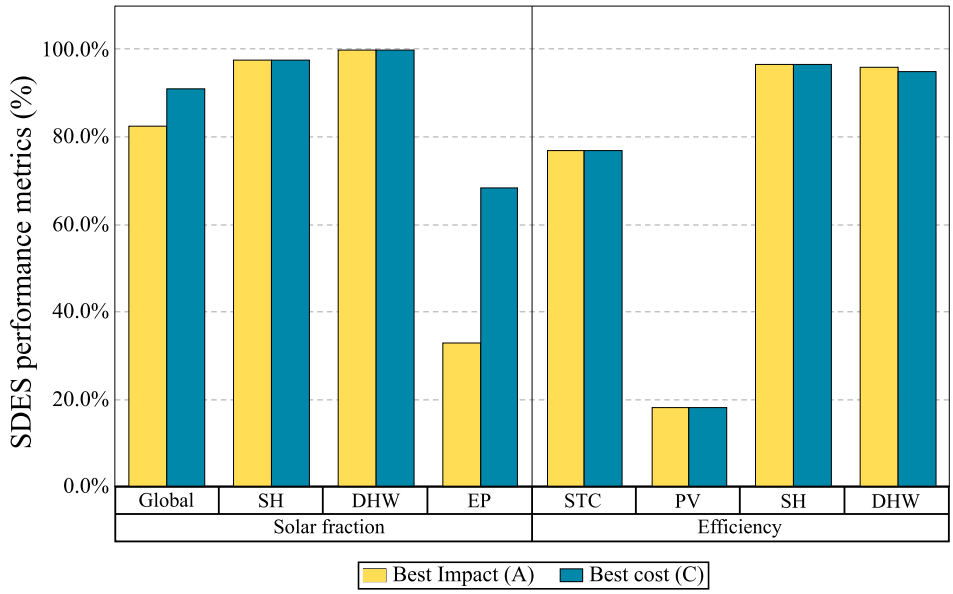

Fig. 8. Solar fraction of the SH, DHW circuits, and electricity production; efficiencies of the STC, PV, SH, and DHW circuits.

primarily attributed to electricity production (EP), as the low-cost solution features a larger PV area, resulting in higher power output rates. The sustainable solution exhibits the EP solar fraction of 32.9 %, while the cost-effective approach demonstrates a remarkable increase of over twofold, reaching 68.5 %. The SH fraction achieves an impressive 97.6 % for both solutions, with DHW approaching almost 100 %. This explains the minimal contribution of SH auxiliary heaters to the overall energy profile of the system, as depicted in Fig. 6, as well as the negligible impact of the DHW heater and heat pump on the system's energy consumption.

In terms of efficiency, the PV, STC, and SH circuits exhibit the same levels of efficiency at 18.3 %, 76.9 %, and 96.6 %, respectively. Additionally, the efficacy of the DHW loop achieves 95.9 % in the context of a sustainable solution and 95 % in a cost-effective scenario.

4.4. Environmental analysis

To facilitate a thorough environmental analysis, Fig. 9 provides a detailed breakdown of the environmental impact contributions from cases A to C for the Pareto optimal solutions over the system's operational lifetime, as well as the baseline solution. The numbers displayed on top of each bar indicate the overall environmental impact measured in ReCiPe points.

As shown in the figure, deploying renewable technologies significantly reduced the ecological damage inflicted on the environment. The baseline scenario acts as a benchmark and is set at 100 %, with a

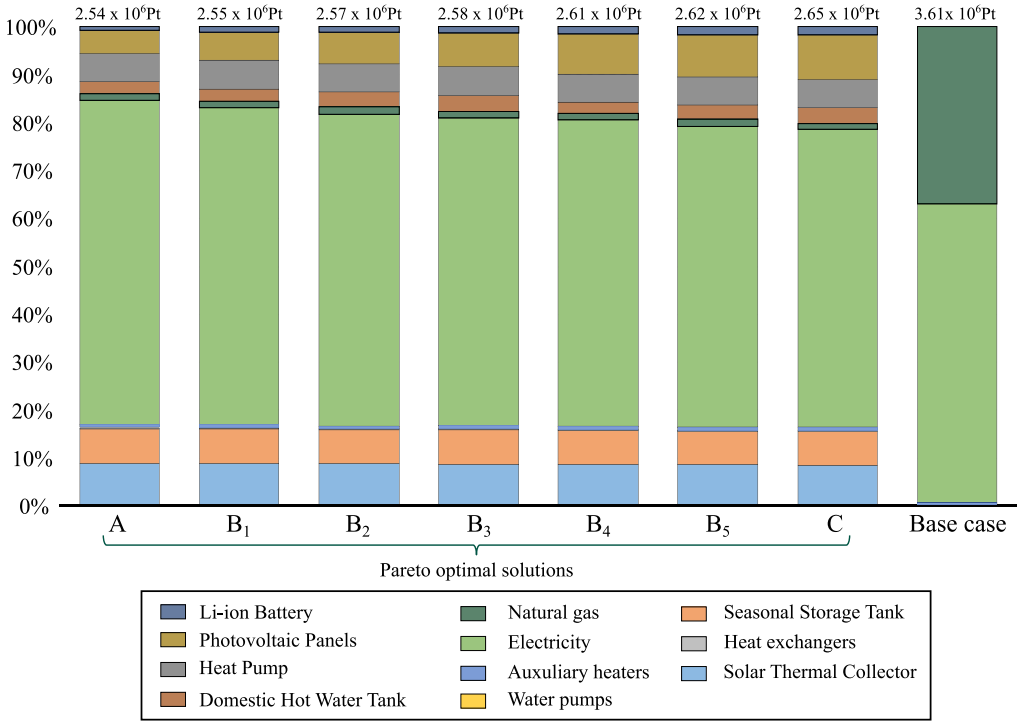

Fig. 9. Environmental analysis of optimal solutions in comparison to the base case.

concerning environmental score of 3.61 × 10^6 Pt. Solution A demonstrates a compelling outcome of 70.2 % (2.54 × 10^6 Pt) compared to the baseline scenario. In contrast, the economically viable solution only results in a modest increase of 4.3 %, bringing the total to 2.65 × 10^6 Pt. Nonetheless, this still represents a more than acceptable result of 73.2 % of the baseline scenario.

In the baseline, electricity accounted for the largest portion of 62.3 % (2.26 × 10^6 Pt), followed by natural gas at 37.1 % (1.34 × 10^6 Pt). The contribution of auxiliary heaters is minimal, accounting for just 0.5 % (1.82 × 10^4 Pt), while the impact of water pumps is negligible, with a mere 1.41 × 10^2 Pt (0.1 %). In contrast, renewable technologies reduced the natural gas impact to an astonishing 1.5 % at its peak, which amounted to no more than 0.39 × 10^5 Pt in the worst-case scenario, showing an outstanding thirty-four-fold decline. The electricity impact showed, albeit more modest but promising results. The total electricity impact after the deployment of renewable technologies accounted for 1.64 × 10^6 Pt, demonstrating a 27 % reduction compared to the base case.

A complete breakdown of environmental analysis for the Pareto optimal solutions and the baseline is provided in the SI (Table 3).

4.5. Economic analysis

This section comprises three subsections: initial investment, operating expenses, and equipment replacement cost. The figures at the apex of each bar, spanning from Fig. 10 to Fig. 13 represent the aggregate (nonspecific) cost, expressed in millions of euros.

4.5.1. Initial investments

The initial investment for the baseline scenario is €667,000; auxiliary heaters constitute the majority of the investment at 79.3 % (€528,900); water pumps account for 7.6 % (€50,700), and a contingency makes up the remaining 13.1 % (€87,000), as depicted in Fig. 10.

In the realm of renewable energy technologies, the initial cost for the most sustainable option reached a staggering €21.7 million, which is 32 times higher than the baseline investment. In comparison, the most cost-effective scenario required an initial investment of €24.3 million, reflecting a 12 % increase and exceeding the baseline investment by more than 36 times.

The main contributors to the initial investment include SST, which accounted for up to 35.4 % or €7.7 million, followed by STC at up to 16.1 % or €3.6 million. Rounding out the top three contributors are heat exchangers, contributing up to 13.9 % or €3.0 million. PV panels represent a more modest cost of €1.54 million (up to 6.3 %); electric batteries cost €2.5 million (up to 10.1 % and HP accounts for 8.1 % (€1.77 million). Contingencies did not exceed 13.1 % (€3.2 million) of the initial cost. A complete breakdown can be found in the SI (Table 4).

4.5.2. Operating costs

Shifting the vector of focus to operating costs (Fig. 11) over the forty-year life cycle of the system, the baseline scenario here exhibited the poorest economic performance when compared to the initial investments. Operating costs in the base scenario total €212.0 million, with natural gas accounting for 58.8 % (€124.7 million) and electricity making up 41.1 % (€87.1 million). A minimum of 0.1 % (€200,700) is allocated for maintenance.

The economically feasible scenario achieved a 66.7 % reduction in operating costs, reaching €70.8 million compared to the baseline, while the sustainable solution led to a 9.3 % increase, accounting for €77.4 million. The primary driver of operating cost variation is grid electricity consumption. Solution C, with a larger PV area, reduced grid electricity demand by 11.7 %, resulting in savings of €6.6 million compared to Solution A. Although this solution required a higher initial investment of €2.6 million (rising from €21.7 million to €24.3 million as depicted in Fig. 10), the long-term electricity cost savings outweighed the upfront expense. Ultimately, this led to a net financial benefit of €4.0 million, making the system with increased PV capacity the more cost-effective choice.

System maintenance for deployed renewable technologies increased significantly compared to the baseline scenario. It rose from a negligible 0.1 % (€200,700) to as much as 18.7 % (€13.2 million) in scenario C. The decrease in maintenance costs to 15.8 % (€12.2 million) in solution A is mainly attributed to the reduction in PV area when transitioning from the economically attractive (C) to the more sustainable solution (A). Additionally, the maintenance expenses associated with auxiliary heaters are lower than those for renewable energy equipment, which

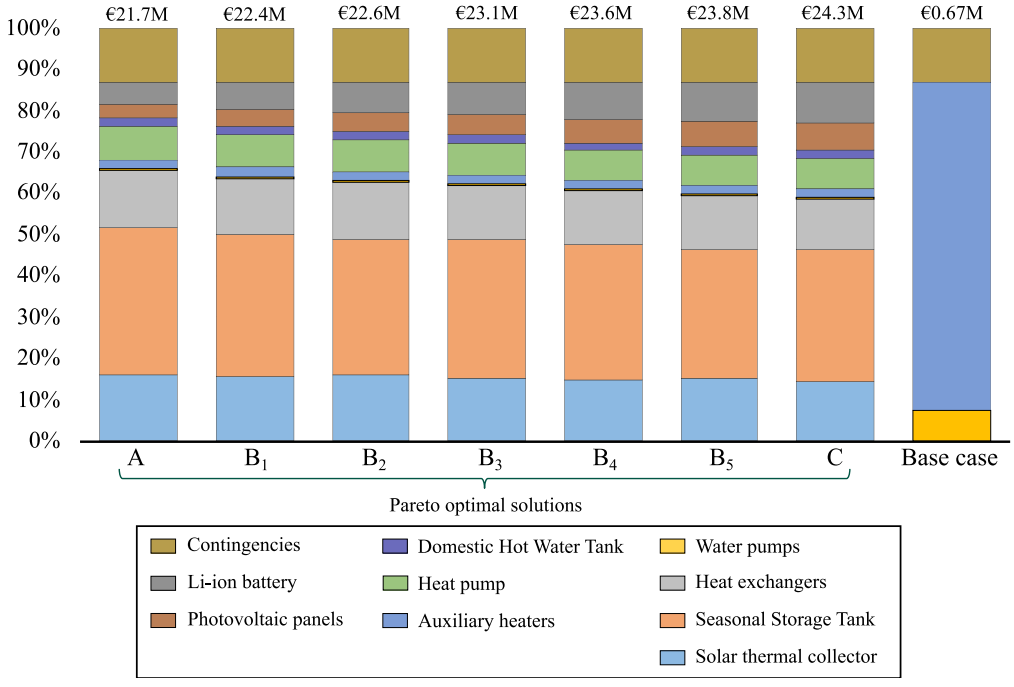

Fig. 10. Capital cost analysis of optimal solutions from the most sustainable to the economically viable solution compared to the base case.

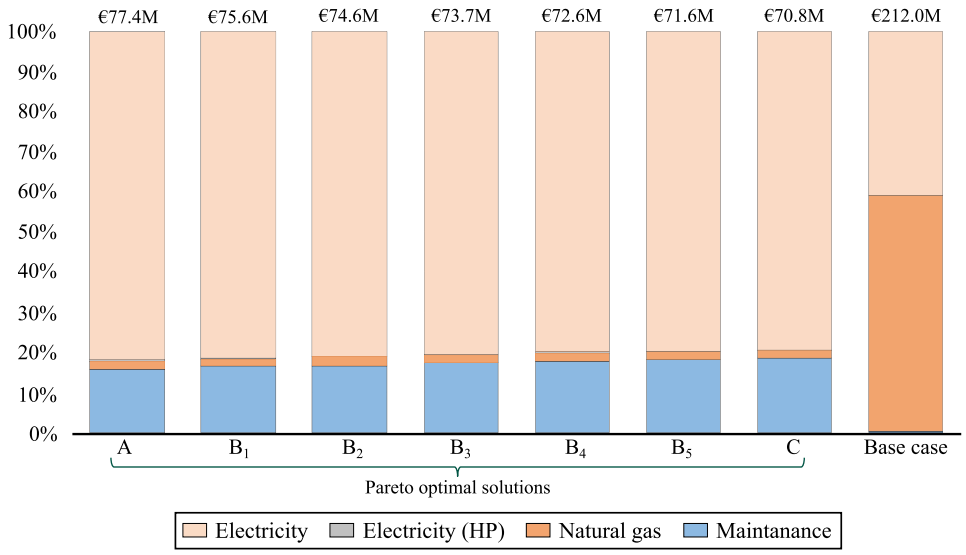

Fig. 11. Operational cost analysis of optimal solutions from the most sustainable to the economically viable solution compared to the base case.

also justifies the reduction of maintenance costs.

Finally, introducing renewable energy reduced natural gas costs by 98.9 %, decreasing from €124.7 million to no more than €1.6 million, and lowering dependence on natural gas from 58.8 % to 2.2 % of total operating costs.

A complete breakdown of operating expenses can be found in the SI (Table 5).

4.5.3. Replacement costs

Replacement costs, as shown in Fig. 12, follow similar trends to the initial investment, indicating that costs increased from the most sustainable to the economically feasible solution. In the baseline scenario, the largest contributors to replacement costs are auxiliary heaters, accounting for 91.3 % (€662,000), followed by water pumps, which made up 8.7 % (€63,500).

In terms of replacement costs for renewable technologies, the top position is held by solar thermal collectors (STC) at 35 % (€4.7 million). This is followed by heat exchangers at 30.1 % (€4.1 million), and heat pump came in third with 17.6 % (€2.4 million). The cost of replacing PV panels does not exceed 14 % (€2.1 million). Additionally, the replacement costs for auxiliary heaters, DHWT, and water pumps are 5 % (€706,000), 4.9 % (€690,000), and 0.5 % (€68,000), respectively. Regarding the replacement of other components, such as SST and electric batteries, they did not need to be replaced at the end of the system's life cycle, as they have not reached the end of their lifespan. The continuous service life of SST is 80 years, while the lifespan of electric batteries is determined by the maximum number of charge/discharge cycles, which averages around 5000 for LFP lithium-ion batteries (see section 3.4).

The total SDES non-specific cost (A1–1, Eq. (A1)) alongside the baseline is presented in Fig. 13. The contribution of each cost (initial investment, operating, and replacement costs) is indicated as a percentage within each bar. A complete breakdown of the replacement and non-specific costs can be found in the SI (Tables 6–7).

4.6. Sensitivity analysis

A sensitivity analysis is conducted to assess the impact of the most critical economic parameters on both the SEC and RCP objective functions. This analysis employs the One-Factor-at-a-Time (OFAT) approach [73], in which each economic parameter is varied from 50 % to 200 %, one at a time, compared to a reference case. Such a broad range has been selected due to the unstable economic situation in the energy sector in recent years [74]. The metrics selected for the sensitivity analysis include the price of electricity, the price of natural gas, and the revenue (electricity selling prices) generated from electricity exported to the grid.

The sensitivity analysis of electricity prices (Fig. 14) demonstrates that the SEC is highly sensitive to grid electricity price variations due to significant electricity consumption, while the RCP remains almost unchanged across all scenarios. A doubling of electricity prices (200 %) leads to a significant increase in SEC, with the cost of the most sustainable solution (A) rising by approximately 38.5 % compared to default prices. However, even in this extreme case, all SDES configurations remain substantially cheaper than the baseline scenario (277 €/MWh), reinforcing the economic feasibility of the system. Furthermore, the ranking of cost-optimal solutions remains consistent – Solution A is always the most expensive, while Solution C is the most cost-effective, regardless of electricity price fluctuations. On the environmental side, RCP values exhibit minimal variation across different electricity prices, demonstrating the system's resilience to market fluctuations. The highest observed difference in RCP across scenarios is

Table 5
Complete breakdown of the operating expenses.

	Solar thermal collector	Heat exchangers	Water pumps	Auxiliary heaters	Heat pump	Domestic Hot Water Tank	Photovoltaic panels
A	4,686,353.971	4,034,419.932	66,707.26057	705,860.7092	2,357,826.6	562,851.4	984,911.8
B1	4,686,353.971	4,034,419.932	66,707.26057	705,860.7092	2,357,826.6	562,851.4	1,251,104
B2	4,781,374.874	4,090,042.909	66,956.03476	705,860.7092	2,357,826.6	648,361.3	1,384,200
B3	4,686,353.971	4,034,419.932	66,707.26057	705,860.7092	2,357,826.6	689,349.7	1,517,297
B4	4,686,353.971	4,034,419.932	66,707.26057	705,860.7092	2,357,826.6	562,851.4	1,783,489
B5	4,781,374.874	4,090,042.909	66,956.03476	705,860.7092	2,357,826.6	648,361.3	1,916,585
C	4,686,353.971	4,034,419.932	66,707.26057	705,860.7092	2,357,826.6	689,349.7	2,049,681
Base case	0	0	63,465.15144	662,016.9616	0	0	0

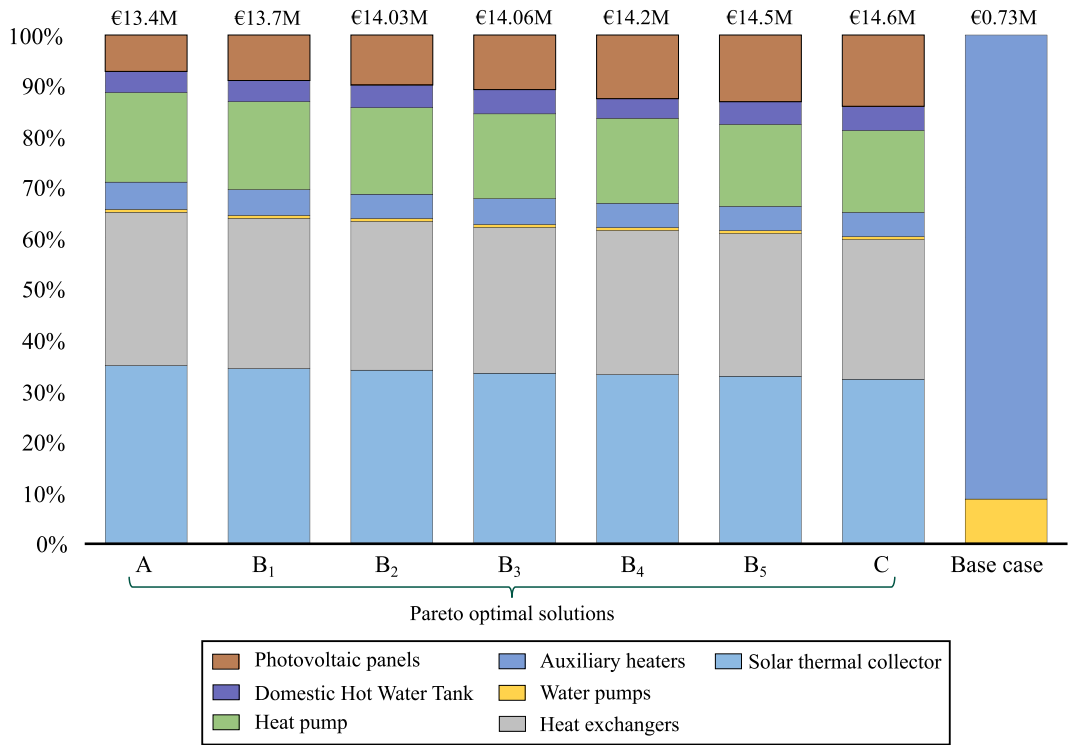

Fig. 12. Replacement cost analysis of optimal solutions from the most sustainable to the economically viable solution, compared to the base case.

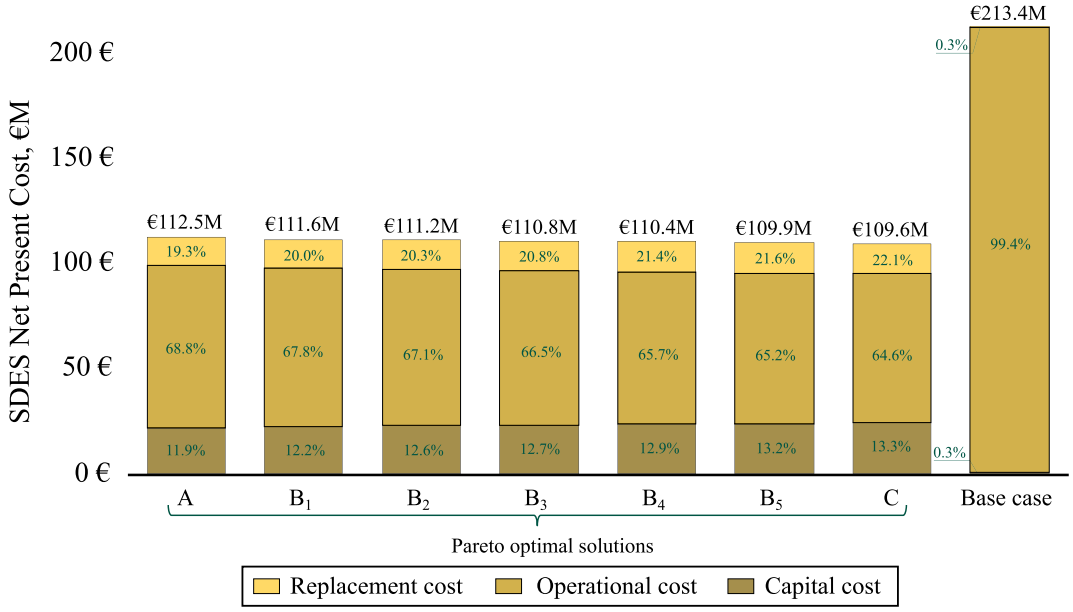

Fig. 13. Net present cost of the solar district energy system and the base case.

Table 6
Complete breakdown of replacement cost.

Case	Capital cost	Operational cost	Replacement cost
A	21,775,749.8	77,361,992.01	13,398,931.71
B1	22,372,763.62	75,569,376.88	13,665,124.1
B2	22,604,831.1	74,646,369.4	14,034,622.84
B3	23,078,093.28	73,680,074	14,057,814.78
B4	23,565,908.58	72,607,331.67	14,197,508.86
B5	23,798,140.34	71,592,885.27	14,567,007.6
C	24,271,091.03	70,828,521.09	14,590,199.55
Base case	666,664.3743	212,031,997.4	725,482.113

merely 0.13 Pt/MWh, confirming that deploying SDES ensures superior environmental performance under all electricity price conditions.

The sensitivity analysis on electricity selling prices (Fig. 15) reveals a strong inverse relationship between economic feasibility and environmental impact. A doubling of selling prices (200 %) significantly reduces the SEC by increasing system revenue from grid electricity exports. However, this also triggers a trade-off point (B_3), where the environmental impact increases sharply, implying a substantial expansion of PV and battery capacity. Conversely, at 50 % selling prices, SEC increases due to reduced revenue, making the system less cost-effective. The findings highlight that while higher electricity selling prices enhance

Table 7
Complete breakdown of net present cost.

—	Environmental impact		
	Price 50%	Default price	Price 200 %
A	3.493663493	3.493663493	3.493663493
B1	3.506165787	3.506165787	3.49461306
B2	3.527638759	3.527007537	3.518474742
B3	3.565132238	3.548395533	3.548395533
B4	3.588557277	3.588557277	3.591593841
B5	3.592075038	3.603635643	3.612730585
C	3.619888894	3.640500747	3.640500747
	Specific economic cost		
	Price 50%	Default price	Price 200 %
A	125.8755403	153.5536698	212.9084663
B1	125.0974509	152.4652596	211.5519531
B2	124.295587	151.8163471	209.3616818
B3	124.0385504	151.3253672	208.1593814
B4	123.6940708	151.1328439	208.1115689
B5	123.2369051	150.3594298	206.5289413
C	122.9231886	150.1418139	206.2572574

economic viability, they also promote higher renewable installations, which may introduce additional environmental considerations.

The sensitivity analysis on natural gas prices (Fig. 16) confirms low dependency on fossil fuels in the optimized SDES configurations. While an increase in natural gas prices (200 %) results in a moderate rise in SEC, the impact remains minor compared to electricity price variations. Likewise, environmental performance is largely unaffected, with a maximum deviation of only 0.15 Pt/MWh. Unlike electricity pricing, no structural changes in PV or battery capacity are observed, reinforcing that natural gas pricing has a negligible influence on system design and optimization. These findings demonstrate that SDES remains economically viable and environmentally sustainable even under extreme natural gas price fluctuations.

Overall, the sensitivity analysis highlights the economic and environmental resilience of the optimized SDES under varying energy price conditions. Electricity prices have the strongest influence on system costs, with higher grid electricity prices significantly increasing the SEC, while RCP remains stable. Conversely, higher electricity selling prices improve economic viability by increasing system revenue, though they also encourage larger PV and battery installations, leading to higher environmental impact beyond a trade-off point (B_3). In contrast, natural gas price variations have a minimal effect on both SEC and RCP, confirming the system's low dependency on fossil fuels. Overall, these findings demonstrate that SDES remains cost-effective and environmentally sustainable across a broad range of energy price scenarios, reinforcing its viability as a robust long-term energy solution.

A complete breakdown of the sensitivity analysis can be found in the SI (Tables 8–10).

5. Conclusion

This study developed a comprehensive optimization framework for Solar District Energy Systems (SDES), combining multiple advanced optimization techniques to effectively explore and identify optimal system designs. Furthermore, the framework incorporated an adaptive approach to dynamically highlight the most influential design parameters during the optimization process, enhancing both efficiency and adaptability.

The framework was applied to a real-world residential community in Falset, Spain, demonstrating the ability of SDES to achieve a solar fraction exceeding 90 %, ensuring long-term sustainability with minimal reliance on fossil fuels. The most economically viable configuration

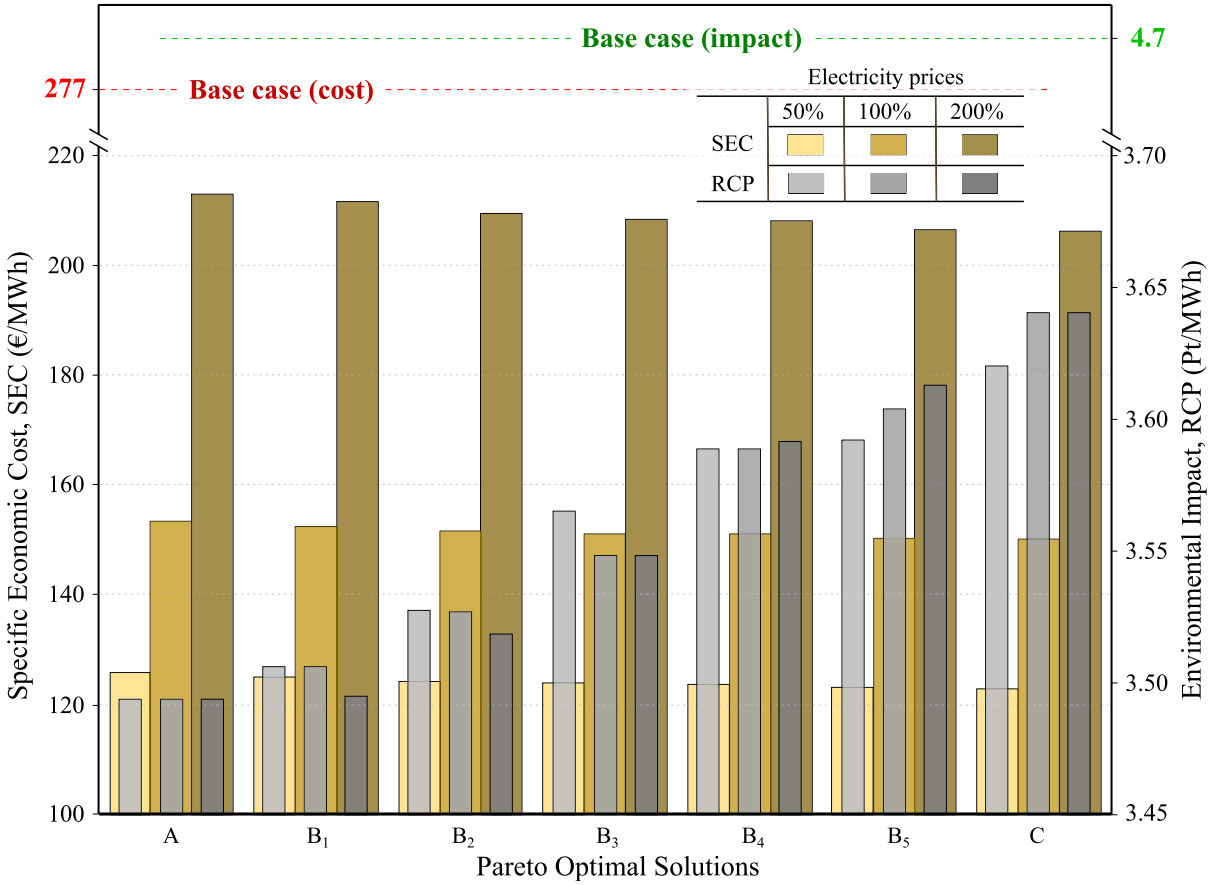

Fig. 14. Sensitivity of SEC and RCP to electricity price changes in optimized SDES configurations.

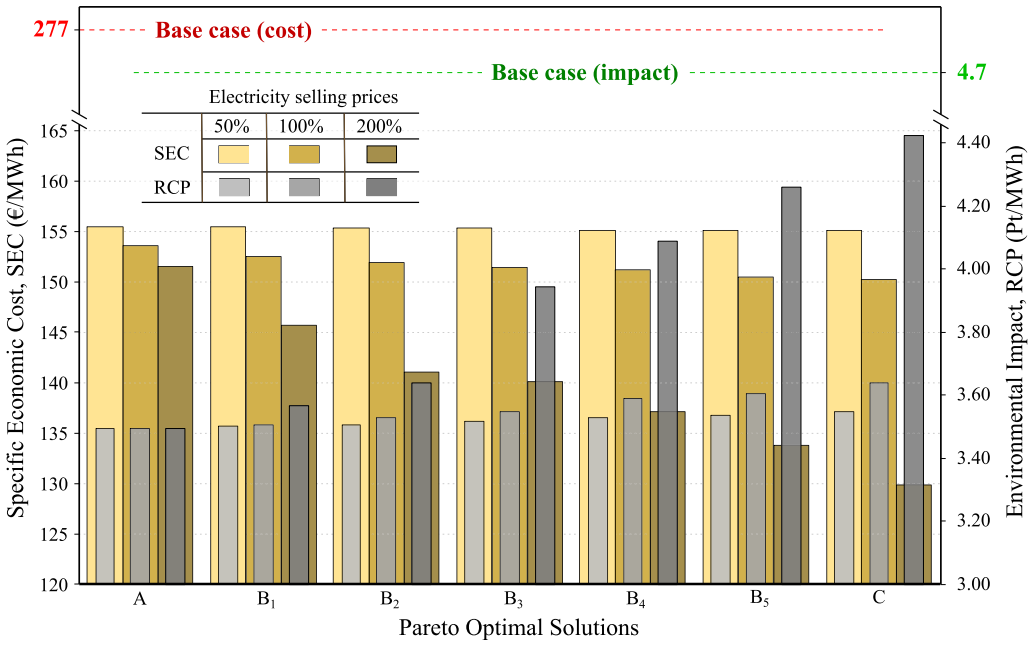

Fig. 15. Sensitivity of SEC and RCP to selling electricity price changes in optimized SDES configurations.

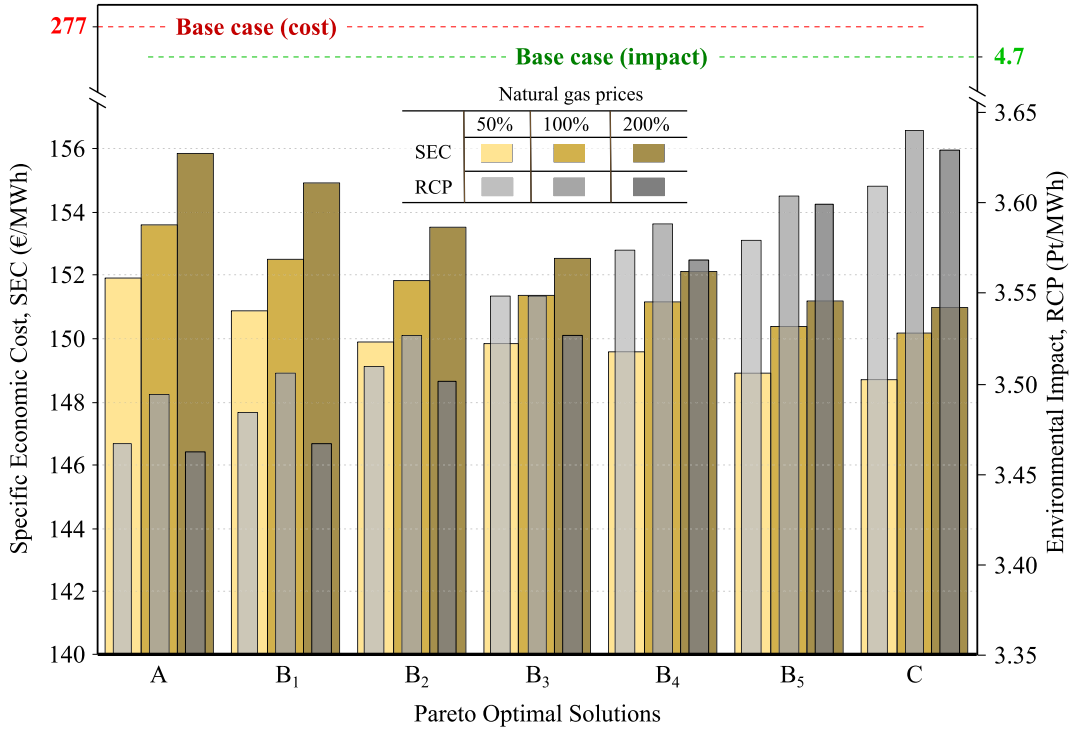

Fig. 16. Sensitivity of SEC and RCP to natural gas price changes in optimized SDES configurations.

reduced operating costs by 66.7 %, reaching €70.8 million compared to the baseline, while the most environmentally optimal configuration reduced impact by 29.8 %, achieving 2.54×10^6 Pt instead of 3.61×10^6 Pt in the baseline scenario. The trade-off between cost efficiency and sustainability was evident, with the cost-optimal solution offering a 2.3 % financial advantage, whereas the environmental-optimal solution provided a 4.1 % improvement in impact reduction.

By combining multiple optimization strategies, the proposed method overcomes the limitations of single-algorithm approaches, avoiding premature convergence while ensuring computational efficiency and scalability. The TRNSYS-Python coupling allowed real-time energy simulations, significantly enhancing the adaptability of the optimization process to diverse system configurations.

The findings provide crucial insights for policymakers, urban planners, and energy system designers considering SDES implementation. The study confirms that solar-driven district energy systems are not only technically feasible but also economically competitive in regions with supportive electricity pricing policies and incentive mechanisms.

The results highlight that grid electricity prices and electricity selling policies significantly impact SDES feasibility, whereas natural gas price

fluctuations have a negligible effect due to minimal fossil fuel reliance. Thus, effective surplus energy trading mechanisms and flexible energy tariffs are key enablers for SDES success.

For decision-makers, the study provides a roadmap for component sizing, ensuring optimal configurations that balance both economic viability and environmental impact. The ability to adapt system configurations dynamically makes SDES a viable alternative to conventional fossil-fuel-based district heating, especially in Mediterranean and temperate climates.

Nomenclature

BMF_k	bare module factor of the equipment unit k
CAP_k	design variable of equipment unit k
C	specific water heat capacity (J/kg ^{o}C)
C_I	initial investment (€)
C_O	operational cost (€)
C_R	replacement cost (€)
Con_{SST}	purchase cost of the construction material of the seasonal storage tank (€)
DVE_k	the design variables for equipment k
FBM_k	bare module factor of the equipment unit k
FID_d	final impact of the damage category d
f_h	fraction concerning the daily total domestic hot water demand (−)
$f_c(x)$	original objective function (RCP or NPC)
Ins_{SST}	purchase cost of the insulation material of the seasonal storage tank (€)
m	total number of equality constraints
n	total number of design variables constraints
P	water pump
PCE_k	capital expenditures of acquired unit k
Pop	population per municipality (number of people)
p	total number of inequality constraints
PW_{AUX}	cost of natural gas consumption (€)
PW_{APP}	cost of electricity purchased from the grid (€)
PW_{HP}	cost of natural gas consumption (€)
PW_M	annual maintenance cost (€)
PVF_n	the present value factor of future cash flow at year n
Q_{DHW}	daily domestic hot water demand (J)
RCP	ReCiPe 2016 aggregated impact factor (Pt/MWh)
T_{sup}	hot water supply temperature (°C)
T_w	tap water temperature (°C)
V	domestic hot water volume per person per day (m^3)
$Year\ A$	base year
$Year\ B$	installation year

Greek symbols

α_{CF}	Contingency factor
α_k	purchase cost coefficient of equipment unit k
β_k	purchase cost exponent of equipment unit k
δ_d	normalization factor for damage category d
ε_d	weighting factor for damage category d
ρ	water density (kg/m^3)

Indices

d	damage category
k	equipment unit

CRediT authorship contribution statement

Ruslan Kotegov: Writing – original draft, Visualization, Software, Methodology, Investigation, Formal analysis. **Mohamed Abokersh:** Validation, Resources, Methodology. **Carles Mateu:** Writing – review & editing, Methodology, Conceptualization. **Adedamola Shobo:** Writing – review & editing, Resources. **Dieter Boer:** Writing – review & editing, Validation, Supervision, Project administration, Funding acquisition, Data curation, Conceptualization. **Manel Vallès:** Writing – review & editing, Validation, Supervision, Project administration, Funding acquisition, Data curation, Conceptualization.

Declaration of competing interest

The authors declare the following financial interests/personal relationships which may be considered as potential competing interests: Manel Valles reports financial support was provided by Ministry of Science, Innovation and Universities. If there are other authors, they declare that they have no known competing financial interests or personal relationships that could have appeared to influence the work reported in this paper.

Acknowledgments

The authors would like to acknowledge financial support from the “Ministry of Science, Innovation and Universities” of Spain (PID2021-127713OA-I00, PID2021-123511OB-C31, PID2021-123511OB-C33, PID2021-124139NB-C22 funded by MCIN/AEI/10.13039/501100011033/FEDER, UE & TED2021-129851B-I00 funded by MCIN/EI/10.13039/01100011033 and by the “European Union NextGenerationEU/PRTR) through “Ministry of Science, Innovation and Universities”, Spain - Recovery, Transformation and Resilience Plan; “The European Union – NextGenerationEU”; and “University of Rovira i Virgili”.

Appendix A. Annex

Table of contents

A.1. Data generation for optimization

In this study, the economic aspects of the system are evaluated using Life Cycle Costing (LCC) as described by Tulus et al. [1], based on the methodologies of Duffie and Beckman (2013) [2] and Kalogirou (2009) [3]. Furthermore, the economic potential of the system was assessed by determining the system's ecological footprint using the Life Cycle Assessment (LCA) methodology [4].

A.1.1. Data preparation for the economic analysis

The LLC employs a comprehensive approach to assess the economic viability of the system. It considers not only the initial investment but also ongoing operational expenses (including maintenance costs) and replacement costs. This comprehensive evaluation empowers decision-makers to thoroughly comprehend and assess key economic metrics throughout the lifespan of the system. As a result, they can minimize unnecessary expenditure during the design phase, even if it entails a higher initial investment [5].

In this manner, the LCC is based on the concept of the future value of the system, which includes all future costs discounted to the present value of the system. Thus, the net present cost (NPC) is the product of the initial investment (C_I), operating (C_O), and replacement costs (C_R).

$$NPC = C_I + C_O + C_R \tag{A1}$$

C_I signifies the preliminary financial contribution allocated for the project's initiation, encompassing the expenses associated with the procurement, installation, and transportation of equipment, in addition to allocating provisions for contingencies, and computed as follows:

$$C_I = (1 + \alpha_{CF}) \sum_k (PCE_k \bullet BMF_k) \tag{A2}$$

where PCE_k accounts for the capital expenditures of acquired unit k, BMF_k is the bare module factor, which includes installation and shipping costs of unit k, and α_{CF} donates for the contingency factor. PCE_k retrieved the initial purchased cost from the base year (Year A) to the year of installation (Year B) based on the Chemical Engineering Plant Cost Index (CEPCI) using the following equation:

$$PCE_k = PCE_k^{year\ A} \bullet \frac{CEPCI^{year\ B}}{CEPCI^{year\ A}} \tag{A3}$$

The initial purchase cost of the unit k at year A can be estimated with the following equations:

$$PCE_k^{year\ A} = \alpha_k \bullet DVE_k^{\beta_k} \forall k = COL, DHW, AUX, BAT \tag{A4}$$

$$PCE_k^{year\ A} = DVE_k^{\beta_k} \bullet 10^{\left[\alpha_k \left(log_{10}(DVE_k)\right)^{\beta_k}\right]} \forall k = HE_1, HE_2, HE_3 \tag{A5}$$

$$PCE_k^{year\ A} = \alpha_k \bullet ln\left(\frac{DVE_k}{1000}\right) + \beta_k \forall k = P_1, P_2, P_3, P_4 \tag{A6}$$

$$PCE_k^{year\ A} = Ins_{SST} + Con_{SST} \forall k = SST \tag{A7}$$

where

$$Ins_{SST} = \alpha_k \bullet DVE_k^{\beta_k} \forall k = XPS, MW, FG \tag{A8}$$

$$Con_{SST} = \alpha_k \bullet DVE_k^{\beta_k} \forall k = NC, HPC \tag{A9}$$

$$Con_{SST} = \alpha_k \bullet e^{\left(\frac{\beta_k}{10^5 DVE_k}\right)} \forall k = UHPC \tag{A10}$$

Here, α_k and β_k represent the parameters for purchasing cost of equipment or materials, and DVE_k denotes the design variables for equipment k. The optimization process considered independent design variables such as solar thermal collector (STC) area (A_{STC}), Seasonal storage (SST) and Domestic hot water (DHWT) tank volumes (V_{SST}, V_{DHWT}), the PV panels area (A_{PV}), and the battery capacity (CAP_{BAT}). Their optimization ranges are determined by generating a feasible set of scenarios using the TRNSYS model, these scenarios are used to obtain the minimum and maximum size of each system component. Variables such as heat exchangers (HE_1, HE_2, HE_3), and the five water pumps with their respective mass flow rates ($\dot{m}_1, \dot{m}_2, \dot{m}_3, \dot{m}_4, \dot{m}_5$) along with the Heat Pump (HP) and the Auxiliary Heaters (AUX_1, AUX_2), are categorized as dependent, with their specifications fine-tuned in line with electricity, space heating, and domestic hot water demands, all dependent on the primary design variables through specific mathematical formulations. The remaining variables, including the insulation types for SST (XPS, MW, FG, indicating extruded polystyrene, mineral wool, and foam glass gravel) and its construction materials ($NC, HPC, UHPC$, denoting normal concrete, high-performance concrete, and ultra-high-performance concrete), are predetermined as per the study by Abokersh et al. [6].

C_O encompasses the annual maintenance of equipment, in addition to the costs of electricity and natural gas for auxiliary gas boilers, determined as follows:

$$C_O = PW_M + PW_{APP} + PW_{AUX} + PW_{HP} \tag{A11}$$

where

PW_M – annual maintenance cost, €.
PW_{APP} – cost of electricity purchased from the grid, €.
PW_{AUX} – cost of natural gas consumption, €.
PW_{HP} – cost of natural gas consumption, €.

The replacement of major equipment during the life of the SDES is accounted for by C_R, including STC, DHWT, PV, lithium iron phosphate (LFP) batteries, heat exchangers (HEs), AUXs, and water pumps. The calculation of C_R is as follows:

$$C_R = PVF_n \sum_k (PCE_k \bullet BMF_k) \tag{A12}$$

where

PVF_n – the present value factor of future cash flow at year n.

PCE_k, BMF_k – the same as in Eq. (A2).

It is also imperative to acknowledge that, in contrast to the remaining equipment, the life cycle of an LFP Li-ion battery is characterized by the total number of cycles (see Section 3.4), as opposed to the estimated Mean Time Between Failures (MTBF) or Estimated Continuous Operation Time (ECOT). Consequently, during the life cycle of a system, a battery requires replacement solely if the number of cycles has surpassed a critical value and the battery has experienced a substantial decline in capacity.

The economic parameters of SDES equipment can be found in section 3, entitled “Case Study”.

A.1.2. Data preparation for environmental analysis

The environmental analysis of the SDES was conducted using the LCA methodology. The LCA is a method of evaluating the environmental impact of a product or system throughout its lifecycle, from its production to its operation. The present study adopted a “cradle-to-grave” approach, excluding end-of-life disposal and recycling due to their minimal and uncertain impact compared to production and usage [7].

The data utilized in this analysis were obtained from reliable databases, such as Ecoinvent [8], and encompassed material inputs, energy consumption, transportation, and operational impacts of pivotal components, including STCs, PVs, HP, battery, and along the SST and DHWT. The environmental impacts were categorized using the ReCiPe 2016 framework, which calculates an aggregated metric (RCP) to represent the system’s overall impact. This metric integrates factors such as resource depletion and ecological effects, normalized to European standards.

By focusing on the main components and their lifecycles, this approach ensures a clear and comprehensive assessment of the SDES’s environmental performance while providing actionable insights for optimizing its design. The RCP can be expressed as follows:

$$RCP = \sum_d \delta_d \bullet \varepsilon_d \bullet FID_d \forall d \tag{A13}$$

where

ε_d, δ_d – specific weighting and normalization factors.

FID_d – final impact of the damage category d.

The weighting factors are derived from the guidelines outlined in the ReCiPe 2016 framework [9], while the normalization factors are derived from the impacts of material extraction and land use in Europe [10].

The environmental impact of SDES components and materials is also addressed in the “Case Study” section.

References

Tulus V, Boer D, Cabeza LF, Jiménez L, Guillén-Gosálbez G. Enhanced thermal energy supply via central solar heating plants with seasonal storage: A multi-objective optimization approach. Appl Energy 2016;181:549–61. Doi: https://doi.org/10.1016/j.apenergy.2016.08.037.

Duffie JA, Beckman WA. Solar engineering of thermal processes. Wiley; 2013.

Kalogirou S. Solar Energy Engineering: Processes and Systems. 2009.

Guillen-Gosalbez G, Caballero J x. A, Esteller LJ, Gadalla M. Application of life cycle assessment to the structural optimization of process flowsheets. Computer Aided Chemical Engineering 2007;24. Doi: https://doi.org/10.1016/S1570-7946(07)80218-5.

Gluch P, Baumann H. The life cycle costing (LCC) approach: A conceptual discussion of its usefulness for environmental decision-making. Build Environ 2004;39. Doi: https://doi.org/10.1016/j.buildenv.2003.10.008.

Abokersh MH, Gangwar S, Spiekman M, Vallès M, Jiménez L, Boer D. Sustainability insights on emerging solar district heating technologies to boost the nearly zero energy building concept. Renew Energy 2021;180:893–913. Doi: https://doi.org/10.1016/j.renene.2021.08.091.

Nemerow NL, Agardy FJ, Sullivan P, Salvato JA. Environmental Engineering: Environmental Health and Safety for Municipal Infrastructure, Land Use and Planning, and Industry: Sixth Edition. 2009. Doi: https://doi.org/10.1002/9780470432822.

Ecoinvent. Ecoinvent database v3. EcoInvent v391 2023;3.

Tulus V, Abokersh MH, Cabeza LF, Vallès M, Jiménez L, Boer D. Economic and environmental potential for solar assisted central heating plants in the EU residential sector: Contribution to the 2030 climate and energy EU agenda. Appl Energy 2019;236:318–39. Doi: https://doi.org/10.1016/j.apenergy.2018.11.094.

JRC European commission. ILCD Handbook: Recommendations for Life Cycle Impact Assessment in the European context. 2011.

A.2. Model setup and input data

A.2.1. Simulation model

The information flow diagram is shown in Fig. A1 (Type – inside TRNSYS GUI). Each component in the model is accompanied by information boxes detailing specific parameters and input-output variables.

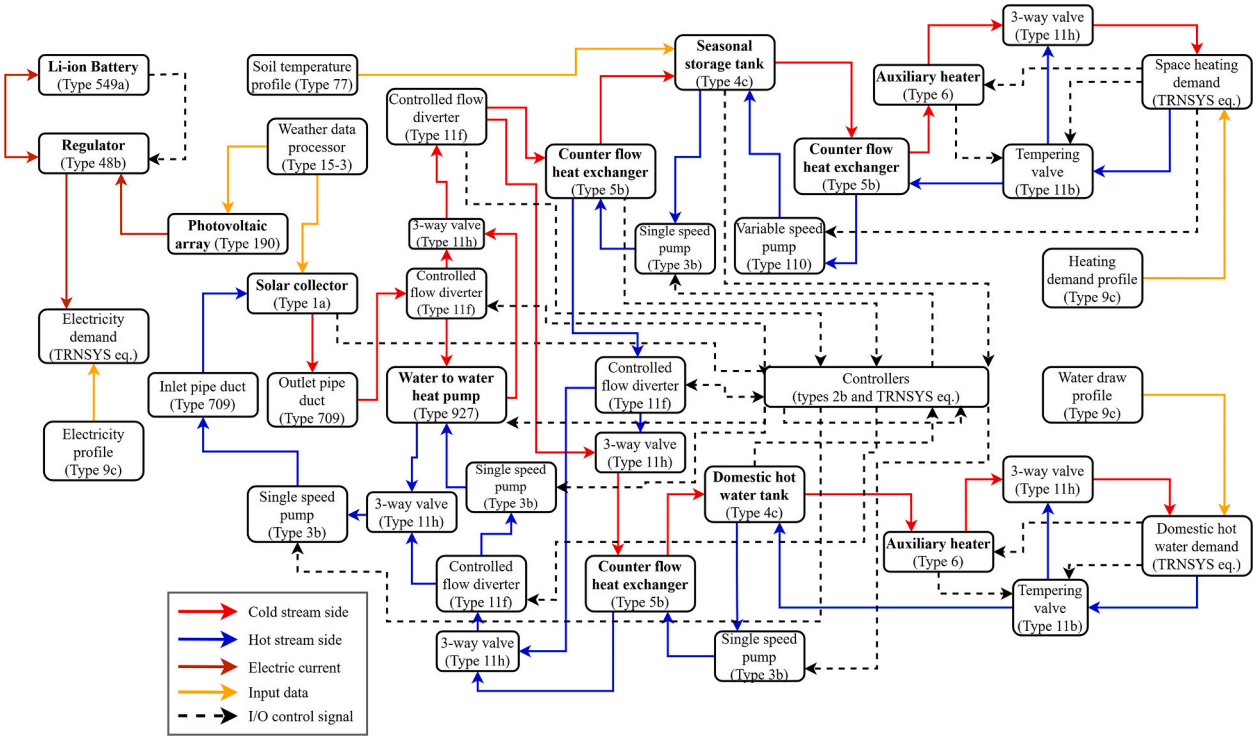

Fig. A1. Flow diagram of the SDES system simulated, with the components and their interconnections using TRNSYS 18.

The model's prime components are listed in Table A1.

Table A1
SDES' main components.

Component	Type	Description	Key Specifications
STC	Type 1a	Solar collectors for capturing thermal energy.	Optical efficiency: 0.817, Heat loss coefficient: 2.205 W/m^2·K
PV	Type 190	Photovoltaic panels for converting solar energy to electricity.	Conversion efficiency: 0.186
Li-Ion battery	Type549a	Li-Ion battery for storing electricity	Discharge curve c-rate: 0.2
Water-to-Water HP	Type 927	Heat pumps use water sources for heating and cooling.	Data from WSHP-PRC026G-TRANE, Heat capacity and power consumption across various temperatures
Stratified Storage Tanks	Type 4c	Fully stratified tanks for storing heated water.	DHWT heat loss coefficient: 0.3125 W/m^2·K, SST heat loss coefficient depends on construction material
Counterflow HEs	Type 5b	Heat exchangers for transferring thermal energy between fluids.	Heat transfer coefficient: 3.931 W/m^2·K
AUXs	Type 6	Backup heaters to supplement the solar thermal system.	Efficiency: 93 %
Centrifugal Pumps	Type 3b	Single-speed pumps for circulating water.	–
Inlet and Outlet Pipe Ducts	Type 709	Ducts for directing flow into and out of system components.	–
Regulator / Inverter	Type 48b	Distributes DC power from the solar cell array to and from a battery	Regulator efficiency: 95 % Inverter efficiency: 96 %
Three-Way Valves	Type 11 h	Valves to control the direction of flow in the system.	–
Controlled Flow Diverters	Type 11f	Devices for managing flow rates within the system.	–
Tempering Valves	Type 11b	Valves for mixing hot and cold water to achieve desired temperatures.	–
Soil Temperature Profiles for SST	Type 77	Soil temperature data to inform SST heat loss calculations.	–
Weather Data	Type 15–3	External weather data for modeling system performance under varying conditions.	–
Time-Dependent Forcing Functions	Type 9c	Profiles for heating and DHW demand over time.	–
Controllers	Type 2b	Devices to control the operation of various system components.	–

The thermal behavior of fluid-filled sensible energy storage tanks (Type 4c) is modeled by dividing the tank into up to 100 fully mixed, equal-volume segments to capture thermal stratification effects. The level of stratification is determined by the number of segments, N, with ($N \leq 100$). N equal to 1 represents a fully mixed tank, where stratification is absent. In this study, the tank is divided into 12 segments (nodes) to adequately account for stratification. The stratified tank design in this Type 4 configuration includes variable inlet positions, allowing incoming fluid to enter at a temperature closely aligned with its own. Uniform heat loss is assumed across all tank nodes.

PV panels (Type 190) generate electricity, with any surplus energy being stored in LFP Li-ion batteries (Type 549a) or injected back into the grid. The operation of the batteries is managed by a regulator/inverter (Type 48b), which monitors the current state of charge (SOC) of the batteries. This

system distributes the load and automatically selects the appropriate operating mode as needed (see section 3.2.1).

A.2.2. System validation

The developed SDES model is implemented in TRNSYS 18, a widely used dynamic simulation software for renewable energy systems and district energy networks. Since the proposed system has not been physically deployed, it is not possible to directly validate the full system. However, the model is built entirely using pre-validated TRNSYS default Types, which have undergone extensive testing and validation against experimental data, manufacturers' specifications, and literature sources. This component-based validation approach ensures that each subsystem operates within established performance limits and has been adopted in many studies [1]. As a result, the overall system can be considered intrinsically validated, following a well-established methodology in energy system modeling. This process ensures that assembling individually validated components maintains the reliability of the complete model [2].

A.2.3. Economic and environmental input data

The parameters for the LCC assessment are outlined in Table A2. Following the referenced guidelines [3], the maintenance cost is estimated to be 1.5 % of the initial purchase cost of the equipment. The prices for natural gas and electricity are €0.0878 and €0.2454 per kWh, respectively, based on data from EUROSTAT [4] and Red Eléctrica [5]. Additionally, the price for electricity injected into the grid is €0.086 per kWh [5]. The inflation rates for natural gas and electricity are 1.64 % and 1.44 %, respectively [4,6]. For the proposed system, the overall inflation rate throughout its lifetime is set at 2.63 %, with a discount rate of 0.32 % [7,8].

Table A2
The economic parameters of SDES equipment [3,9].

Equipment, material	Options	α_k	β_k	CAP_k	Unit	Base year	FBM_k
STC		974.2	0.8330	Aperture area	m^2	2007	1
PV		190.92	1	Aperture area	m^2	2022	1
Li-ion battery		191.0	1	Weight	kg	2023	3.31
HP		2053.8	−0.3480	Duty	kW	2014	1.4
DHWT		11,680	−0.5545	Volume	m^3	2018	1
AUX		225.0	0.7460	Duty	kW	2001	2.1
HE		3.133	−0.331	Exchange area	m^2	2001	3.29
Pump (P_1, P_2, P_4, P_5)		389.0	283.15	Mass flow rate	kg/h	2009	3.24
Pump (P_3)		389.0	717.0	Mass flow rate	kg/h	2009	3.24
SST insulation	XPS	561.09	0.3974	Material thickness	m	2017	1
	MW	1902.7	0.942	Material thickness	m	2017	1
	FG	311.41	0.9698	Material thickness	m	2014	1
SST construction	NC	4178.1	−0.394	Volume	m^3	2000	1
	HPC	2575	−0.363	Volume	m^3	2004	1
	UHPC	90.83	−3	Volume	m^3	2004	1

The input parameters for the LCA were obtained from the Ecoinvent v. 3.10.1 database [10]. This database categorizes the environmental damage associated with the components of the SDES using the Recipe 2016 methodology. The cumulative endpoint environmental impact is calculated using Eq. (A13), and the specific impacts of the different components of the SDES are presented in Table A3.

Table A3
The environmental impact of SDES equipment based on ReCiPe 2016 [10].

Equipment/material	Options	Impact factor (ReCiPe 2016)	Unit
STC		9.96	Pt/m^2
PV		15.2	Pt/m^2
LFP Li-ion battery		2.05	Pt/kg
HP		6.66	Pt/kW
DHWT		41.82	Pt/m^3
AUX		4.0	Pt/kW
HE		$6.64 \cdot 10^{-2}$	Pt/m^2
Water pump		4.42	Pt/kW
SST insulation	XPS	0.853	Pt/kg
	MW	$2.86 \cdot 10^{-3}$	Pt/kg
	FG	0.162	Pt/kg
SST construction	NC	$6.1 \cdot 10^{-3}$	Pt/kg
	HPC	$2.75 \cdot 10^{-3}$	Pt/kg
	UHPC	0.015	Pt/kg
Natural gas		$2.8 \cdot 10^{-3}$	Pt/kWh
Electricity		$12.5 \cdot 10^{-3}$	Pt/kWh

References

Calise F, Cappiello FL, Cimmino L, Vicidomini M, Petrakopoulou F. Thermoeconomic analysis of a novel topology of a 5th generation district energy network for a commercial user. Appl Energy 2024;371. Doi: https://doi.org/10.1016/j.apenergy.2024.123718.

Ceglia F, Marrasso E, E> CR, Sasso M. Small Renewable Energy Community: The Role of Energy and Environmental Indicators for Power Grid 2021. Doi: https://doi.org/10.3390/su.

Tulus V, Boer D, Cabeza LF, Jiménez L, Guillén-Gosálbez G. Enhanced thermal energy supply via central solar heating plants with seasonal storage: A multi-objective optimization approach. Appl Energy 2016;181:549–61. Doi: https://doi.org/10.1016/j.apenergy.2016.08.037.

European Union | Eurostat. Statistics | Eurostat n.d. https://ec.europa.eu/eurostat/ (accessed October 9, 2023).

Red Electrica. Home | Red Eléctrica n.d. https://www.ree.es/en (accessed October 9, 2023).

Trading Economics. EU Natural Gas TTF - Price - Chart - Historical Data - News n.d. https://tradingeconomics.com/commodity/eu-natural-gas (accessed October 9, 2023).

European Commission. Reference and discount rates - European Commission n.d. https://competition-policy.ec.europa.eu/state-aid/legislation/reference-discount-rates-and-recovery-interest-rates/reference-and-discount-rates_en (accessed October 9, 2023).

WorldData Info. Inflation rates in Spain n.d. https://www.worlddata.info/europe/spain/inflation-rates.php (accessed October 9, 2023).

Cellura S, Mazza A, Bompard E, Corgnati S. An Extended Approach to the Evaluation of Energy Storage Systems: A Case Study of Li-Ion Batteries. Electronics (Switzerland) 2023;12. Doi: https://doi.org/10.3390/electronics12112391.

Ecoinvent. Ecoinvent database v3. EcoInvent v391 2023;3.

A.3. Optimization metrics and model performance evaluation

A.3.1. Model configuration

In the development of the predictive model and the subsequent analysis of decision-making, a carefully balanced approach was adopted to take into account environmental and economic considerations. The technique of TOPSIS (Technique for Order Preference by Similarity to Ideal Solution) was employed, in which the environmental impact and the economic cost were assigned weights ranging from zero to one, as illustrated in Table A4.

Table A4
TOPSIS weights for environmental and economic indicators.

Indicator	Applied weights						
	A	B_1	B_2	B_3	B_4	B_5	C
Environmental impact (RCP)	100.00 %	82.00 %	64.00 %	46.00 %	28.00 %	10.00 %	0.00 %
Specific economic cost (SEC)	0.00 %	18.00 %	36.00 %	54.00 %	72.00 %	90.00 %	100.00 %

For predictive accuracy, the Gradient Boosting Regressor (GBR) was fine-tuned with hyperparameters listed in Table A5.

Table A5
Hyperparameters for gradient boosting regressor model.

Applied regression	Gradient Boosting Regressor							
Model parameters	Random state	N° estimators	Learning rate	Max depth	Min samples split	Validation fraction	N° no change iterations	Tolerance
	0–99,999	50	0.01	2	2–10 %	0.1	10	0.0001

To ensure the model's resilience and overfitting prevention, a k-fold cross-validation technique was adopted, employing shuffled data partitions and added noise, significantly enhancing the accuracy of the model's predictions (Table A6).

Table A6
k-fold cross-validation configuration.

k-fold cross-validation				
N folds (splits)	Number of runs	Shuffle	Noise	Random state
6–14	1–7	TRUE	TRUE	0–99,999

Randomization incorporation and perturbations guaranteed that cross-validation not only rigorously evaluated the model across diverse subsets of data but also scrutinized its proficiency in practical, real-life situations where data may lack ideal perfection. The dynamic nature of the model enabled it to adjust and automatically determine the optimal number of folds and iterations (runs), resulting in high accuracy that is contingent upon the data behavior.

A.3.2. Model performance evaluation

In this study, a model based on Feature Importance Scoring (FIS) was accepted as an optimization framework. When designing complex and intricate systems, it was central to comprehend the relative significance of each system component upon others. In other words, it was essential to ascertain the influence of alterations in individual components of a system on the model's convergence toward the global optimum at the earliest stages (exploration). On the other hand, manipulation of other parameters proved particularly advantageous during the local search (exploitation). Exploration prevented premature convergence by discovering new regions of the solution space, whereas exploitation ensured that the solutions within a given area were meticulously scrutinized. Striking a balance between these two processes represented a key challenge in optimization algorithms. This section explored the model's capacity for accurate discrimination between these variables, showcasing its expertise in guiding strategic adjustments that optimized both the environmental performance and economic efficiency of the system.

The process of FIS assessment is instrumental in determining the extent to which each independent variable influences the objective, also known as predictive outcome. Through the training of a regression model on a dataset comprising both design variables (independent variables) and objectives (output data), the model meticulously evaluated the impact of each variable on the predictive process. It is vital to understand that the FIS uses predictions to assess variable influence, but it's not a surrogate model; it simply interprets feature influence within the regression process.

The significance of each feature is quantified as a percentage, reflecting its relative importance in comparison to the other features. These percentages, when considered collectively, provided a comprehensive understanding of which variables exert the most substantial influence on the predictive outcome, with their cumulative sum always amounting to 100 %. Following the evaluation assessment of each design parameter, they are

prioritized in order of importance, ranging from the most to the least important. Each parameter is assigned a numerical value between 1 and N (ranked), where N represents the degrees of freedom or, in other words, the total number of design parameters.

Table A7
Detailed feature importance metrics for RCP and SEC optimization.

Feature	RCP optimization				SEC optimization			
	Train MSE	Test MSE	Prediction error	Rank	Train MSE	Test MSE	Prediction error	Rank
SST Volume	0.02332	0.02346	0.60%	I	0.03128	0.03134	0.19 %	I
PV Area	0.03799	0.03837	1.01 %	II	0.03215	0.03226	0.36 %	III
Battery Cell Capacity	0.03909	0.03956	1.22 %	III	0.03136	0.03145	0.29 %	II
STC Area	0.04117	0.04160	1.06 %	IV	0.04546	0.04556	0.22 %	V
DHWT volume	0.04595	0.04598	0.06 %	V	0.04530	0.04534	0.07 %	IV

Numerous metrics are available for assessing a predictive model's accuracy and dependability. In this investigation, MSE (Mean Squared Error) was employed as one of the most widely recommended metrics, characterized by its reliability, precision, and user-friendliness.

MSE is a unitless metric for assessing the precision of a model's predictions. It represents the average squared difference between the actual values and the predictions made by the model. MSE is calculated individually for the training dataset (used during model learning) and the testing dataset (unseen by the model during training). By comparing the MSE for training and testing, we can evaluate the model's ability to generalize to new data, which in turn indicates the reliability of the feature importance scores.

Table A7 represents the numerical FIS breakdown, such as prediction errors, MSEs, and ranking for RCP and SEC optimization.

Another evaluation criterion is the degree of convergence between the test and train MSEs, as shown in Fig. A2. A small gap between the train and test MSE (the prediction error varies from 0.06 % to 1.22 %) shows good generalization, while a large gap suggests over- or underfitting. The always positive prediction error implies that the train MSE is slightly lower than the test MSE and assumes a slight underfitting. The negligible underfit is preferable since it ensures that the model doesn't overlearn patterns specific to the training data, allowing it to generalize better to unseen data, whereas overfitting (train MSE is higher than test MSE) harms real-world performance.

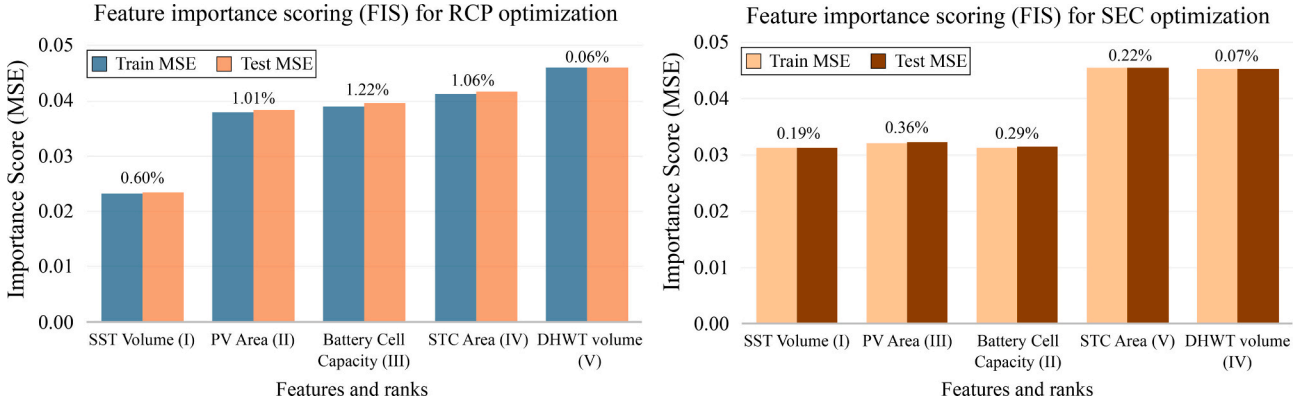

Fig. A2. Feature importance scoring for RCP and SEC optimization.

A.4. Energy dynamics of the SDES

The system's thermal behavior is regulated by an advanced rule-based controller (RBC), while its electrical behavior relies on a controller/inverter (Type 48b) that operates in multiple modes (see Section 3.2.1).

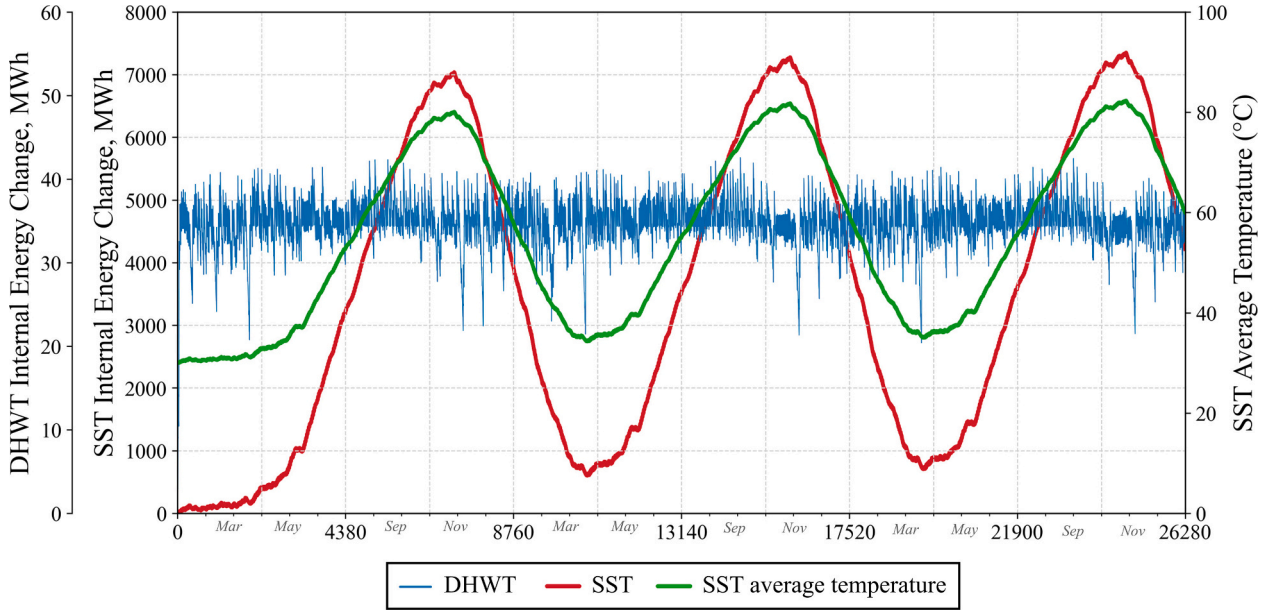

Fig. A3. The three-year energy changes in SST and DHWT using an RBC.

Fig. A3 depicts the thermal energy dynamics of the SDES over a triennial period starting from January 1. The most sustainable solution (A) was selected for visualization as it minimizes environmental impact and reduces gas consumption. Although the collector area varies across solutions, its minor differences (Fig. A3) have a negligible impact on the system's thermal behavior.

The DHWT, serving as a small-scale short-term storage unit, exhibits frequent fluctuations, with its internal energy change varying between 30 MWh and 40 MWh. This behavior reflects its function of meeting daily and short-term thermal demands. The SST energy change follows a seasonal cycle, peaking at 7200 MWh and dropping to 900 MWh in colder months.

The absence of plateaus at peak and trough (depletion) SST levels indicates a balanced system, with an optimally sized STC area and SST volume. The smooth charge-discharge cycles confirm efficient seasonal energy management without overcharging or underutilization, ensuring stable long-term operation.

As far as the electrical performance of the system is concerned, it is shown in Figs. A4 and A5 for typical summer and winter weeks determined following the Contreras-Aguilar et al. methodology [1].

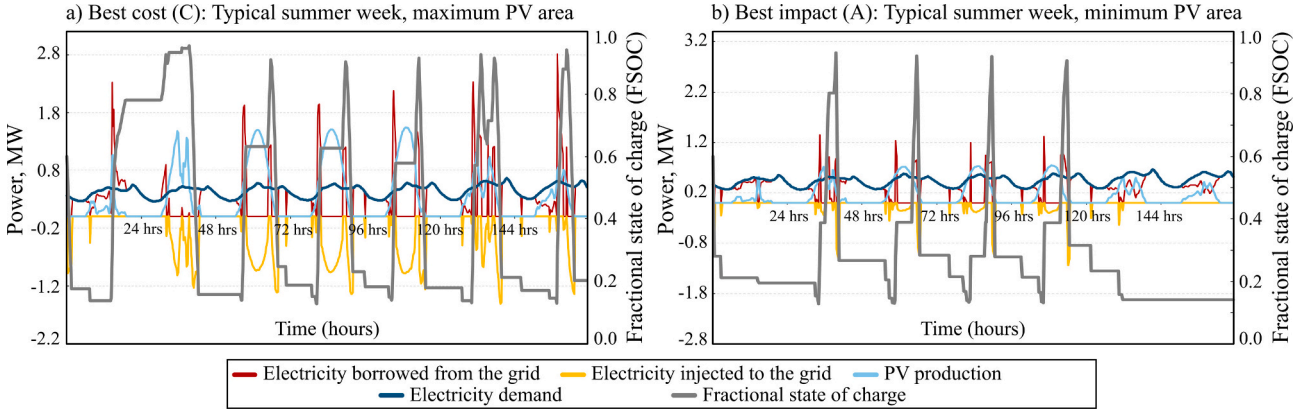

Fig. A4. Electricity flow and battery behavior – typical summer week (August 1 – August 7).

Solution C (Fig. A4-a), with a larger PV area, demonstrates higher PV production, reducing grid dependency and enabling greater electricity injection. This results in a more stable fractional state of charge (FSOC), ensuring efficient battery utilization. In contrast, Solution A (Fig. A4-b), with minimal PV capacity, exhibits lower PV generation, increased reliance on grid electricity, and deeper battery discharges, leading to a less stable FSOC. Overall, Solution C enhances self-sufficiency, minimizing grid interaction while maintaining efficient energy storage and distribution.

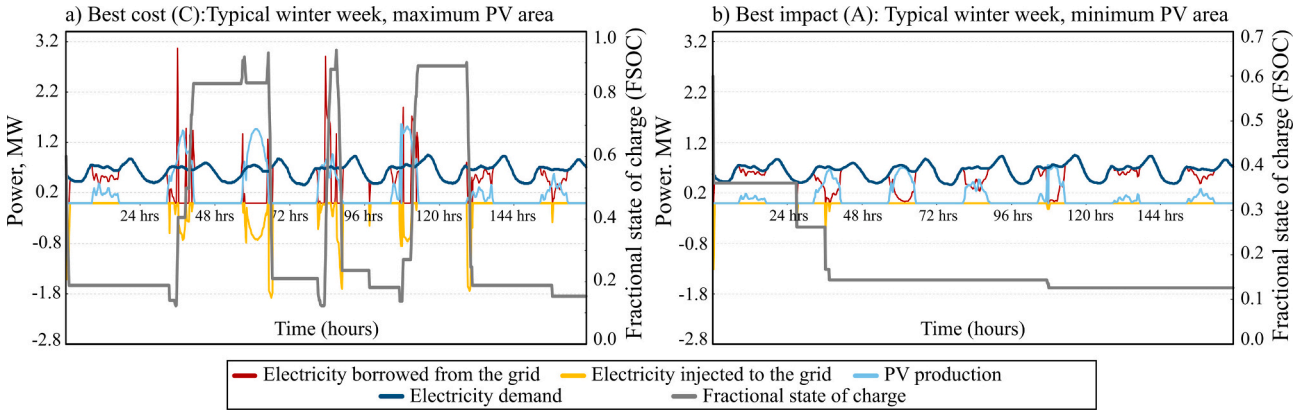

Fig. A5. Electricity flow and battery behavior – typical winter week (January 25 – January 31).

In winter, both solutions exhibit reduced PV production, leading to increased reliance on grid electricity. Solution C (Fig. A5-a) maintains a relatively higher FSOC with occasional battery charging, whereas Solution A (Fig. A5-b) experiences prolonged battery depletion and frequent grid dependency. Unlike summer, where a larger PV area facilitated surplus energy injection, winter conditions result in a deficit-driven operation for both solutions, with minimal energy available for storage or grid export. These findings reflect the seasonal variation in PV availability and its impact on system performance. The behavior of the lithium-ion battery is consistent with the results published in [2].

References

Contreras-Aguilar JA, Gijón-Rivera M, Rivera-Solorio CI, Noh-Pat F. Thermo-economic assessment of a double-layer phase-change material in building roofs in a semi-arid climate. Thermal Science and Engineering Progress 2025;57. Doi: https://doi.org/10.1016/j.tsep.2024.103093.

Haddad M, Javani N, Rezaie B. Energy storage management in a near zero energy building using Li-ion, lead-acid, flywheel, and photovoltaic systems with TRNSYS simulation. Process Safety and Environmental Protection 2025;196. Doi: https://doi.org/10.1016/j.psep.2025.106898.

Data availability

Data will be made available on request.

References

[1] Scott R. The history of the IEA 1974–1994, IEA the first 20 Zears, Vol. II, major policies and actions. 2025.

[2] Green MA, Dunlop ED, Yoshita M, Kopidakis N, Bothe K, Siefer G, et al. Solar cell efficiency tables (version 64). Progress Photovolt Res Appl 2024;32:425–41. https://doi.org/10.1002/pip.3831.

[3] Lund H, Möller B, Mathiesen BV, Dyrelund A. The role of district heating in future renewable energy systems. Energy 2010;35:1381–90. https://doi.org/10.1016/j.energy.2009.11.023.

[4] (UNFCCC) UNFC on CC. Kyoto protocol to the United Nations framework convention on climate change. 1997.

[5] Sandor D. Analysis insights: energy storage - possibilities for expanding electric grid flexibility (brochure), NREL (National Renewable Energy Laboratory). 2025.

[6] Commission E. The European Green Deal – Delivering the EU'S 2030 climate targets. Brussels, Belgium: European Union; 2023. https://doi.org/10.2775/783179.

[7] Commission E. Climate action and the European Green Deal. 2025. https://doi.org/10.2775/189974.

[8] Henning HM, Döll J. Solar systems for heating and cooling of buildings. Energy Procedia 2012;30:633–53. https://doi.org/10.1016/j.egypro.2012.11.073. Elsevier Ltd.

[9] Commission E. Overview of district heating and cooling markets and regulatory frameworks under the revised renewable energy directive main report final version. 2025.

[10] Sibbitt B, McClenahan D, Djebbar R, Thornton J, Wong B, Carriere J, et al. The performance of a high solar fraction seasonal storage district heating system - Five years of operation. Energy Procedia 2012;30:856–65. https://doi.org/10.1016/j.egypro.2012.11.097. Elsevier Ltd.

[11] Barzegkar-Ntovom GA, Chatzigeorgiou NG, Nousdilis AI, Vomva SA, Kryonidis GC, Kontis EO, et al. Assessing the viability of battery energy storage systems coupled with photovoltaics under a pure self-consumption scheme. 2019. https://doi.org/10.1016/j.renene.2020.01.061.

[12] Guelpa E, Verda V. Thermal energy storage in district heating and cooling systems: a review. Appl Energy 2019:252. https://doi.org/10.1016/j.apenergy.2019.113474.

[13] Cole WJ, Powell KM, Edgar TF. Optimization and advanced control of thermal energy storage systems. Rev Chem Eng 2012;28:81–99. https://doi.org/10.1515/revce-2011-0018.

[14] Capone M, Guelpa E, Verda V. Multi-objective optimization of district energy systems with demand response. Energy 2021:227. https://doi.org/10.1016/j.energy.2021.120472.

[15] Talebi B, Mirzaei PA, Bastani A, Haghighat F. A review of district heating systems: modeling and optimization. Front Built Environ 2016:2. https://doi.org/10.3389/fbuil.2016.00022.

[16] Röder J, Meyer B, Krien U, Zimmermann J, Stührmann T, Zondervan E. Optimal design of district heating networks with distributed thermal energy storages – method and case study. Int J Sustain Energy Plan Manag 2021;31:5–22. https://doi.org/10.5278/ijsepm.6248.

[17] Raida Z, Šeděnka V, Raida Z. Critical comparison of multi-objective optimization methods: genetic algorithms versus. Swarm Intellig 2010;19.

[18] Koziel S, Leifsson L. Surrogate-based modeling and optimization: applications in engineeringvol. 9781461475514. New York: Springer; 2013. https://doi.org/10.1007/978-1-4614-7551-4.

[19] Vrugt JA, Robinson BA. Improved evolutionary optimization from genetically adaptive multimethod search104; 2007.

[20] Blackburn L, Young A, Rogers P, Hedengren J, Powell K. Dynamic optimization of a district energy system with storage using a novel mixed-integer quadratic programming algorithm. Optim Eng 2019;20:575–603. https://doi.org/10.1007/s11081-018-09419-w.

[21] Kamerling S, Vuillerme V, Rodat S. Solar field output temperature optimization using a milp algorithm and a 0d model in the case of a hybrid concentrated solar thermal power plant for ship applications. Energies (Basel) 2021:14. https://doi.org/10.3390/en14133731.

[22] Molnar C. Interpretable machine learning A guide for making black box models explainable. 2025.

[23] Sobol IM. Global sensitivity indices for nonlinear mathematical models and their Monte Carlo estimates55; 2001.

[24] Kalkan C, Ward C, Duquette J, Khouli F, Ezan MA. Lessons learned from modelling a complex residential building energy system in TRNSYS. 2025.

[25] Maurice Clerc. Particle swarm optimization. London: ISTE Ltd; 2006.

[26] Huang W, Xu J. Particle swarm optimization. Springer Tracts in Civil Engineering; 2023. https://doi.org/10.1007/978-981-99-2213-0_2.

[27] Loh W-L. On Latin hypercube sampling24; 1996.

[28] Mckay MD, Beckman RJ, Conover WJ. A comparison of three methods for selecting values of input variables in the analysis of output from a computer code42; 2000.

[29] Liberti L, Lavor C, Maculan N, Mucherino A. Euclidean distance geometry and applications. SIAM Rev 2014;56:3–69. https://doi.org/10.1137/120875909.

[30] Mesquita DPP, Gomes JPP, Souza Junior AH, Nobre JS. Euclidean distance estimation in incomplete datasets. Neurocomputing 2017:248. https://doi.org/10.1016/j.neucom.2016.12.081.

[31] Chiu WY, Yen GG, Juan TK. Minimum Manhattan distance approach to multiple criteria decision making in multiobjective optimization problems. In: IEEE Transactions on Evolutionary Computation; 2016. p. 20. https://doi.org/10.1109/TEVC.2016.2564158.

[32] Ribeiro MI. Gaussian probability density functions: Properties and error characterization. 2004.
[33] Saini P, Huang P, Fiedler F, Volkova A, Zhang X. Techno-economic analysis of a 5th generation district heating system using thermo-hydraulic model: a multi-objective analysis for a case study in heating dominated climate. Energ Buildings 2023:296. https://doi.org/10.1016/j.enbuild.2023.113347.
[34] Li T, Wang X, Yu Y, Fu Q, Chen M, Xu C, et al. Performance and PV benefits analysis of multi-source renewable energy systems for different types of buildings on university campus. Renew Energy 2024:237. https://doi.org/10.1016/j.renene.2024.121522.
[35] Liu X, Paritosh P, Awalgaonkar NM, Bilionis I, Karava P. Model predictive control under forecast uncertainty for optimal operation of buildings with integrated solar systems. Solar Energy 2018;171:953–70. https://doi.org/10.1016/j.solener.2018.06.038.
[36] Si Q, Peng Y, Jin Q, Li Y, Cai H. Multi-objective optimization research on the integration of renewable energy HVAC systems based on TRNSYS. Buildings 2023:13. https://doi.org/10.3390/buildings13123057.
[37] Roncal JJ, Rodríguez-Martín J, Muñoz-Antón J, Abanades A, Gurruchaga I, González D, et al. Development of TRNSYS Macros for solar resource integration in a district heating and cooling network. In: W.E. DISTRICT Project. AIP Conf Proc. 2815. American Institute of Physics Inc; 2023. https://doi.org/10.1063/5.0149410.
[38] Wetter M. GenOpt®-A generic optimization program GenOpt Ö-A generic optimization program. 2025.
[39] Cruz AS, Caldas LR, Mendes VM, Mendes JC, Bastos LEG. Multi-objective optimization based on surrogate models for sustainable building design: a systematic literature review. Build Environ 2024:266. https://doi.org/10.1016/j.buildenv.2024.112147.
[40] Brunton SL, Noack BR, Koumoutsakos P. Machine learning for fluid mechanics. Annu Rev Fluid Mech 2020;52:477–508. https://doi.org/10.1146/annurev-fluid-010719-060214.
[41] Klein SA, et al. TRNSYS reference manual. In: Standard Component Library Overview. TRNSYS 16, a TRaNsient SYstem Simulation Program. 3; 2006.
[42] İbrahim Hakan. Tol. TRNSYS from Python. https://github.com/DrTol/TRNSYSfromPython; 2020 (accessed October 9, 2023).
[43] Bauer D, Marx R, Nußbicker-Lux J, Ochs F, Heidemann W, Müller-Steinhagen H. German central solar heating plants with seasonal heat storage. Solar Energy 2010:84. https://doi.org/10.1016/j.solener.2009.05.013.
[44] Tecnalia, Acciona, Dappolonia, Mostostal. Effective integration of seasonal thermal energy storage systems in existing buildings. 2012.
[45] 1.3.5.16. Kolmogorov-Smirnov Goodness-of-Fit Test. https://www.itl.nist.gov/div898/handbook/eda/section3/eda35g.htm; 2025 (accessed October 9, 2023).
[46] Sari F. Forest fire susceptibility mapping via multi-criteria decision analysis techniques for Mugla, Turkey: a comparative analysis of VIKOR and TOPSIS. For Ecol Manage 2021:480. https://doi.org/10.1016/j.foreco.2020.118644.
[47] Statistical Institute of Catalonia. Idescat. Population and Housing Census. Dwellings. By type of dwelling. Falset. https://www.idescat.cat/pub/?id=censph&n=30&geo=mun%3A430555&lang=en; 2025 (accessed October 9, 2023).
[48] Tulus V, Abokersh MH, Cabeza LF, Vallès M, Jiménez L, Boer D. Economic and environmental potential for solar assisted central heating plants in the EU residential sector: contribution to the 2030 climate and energy EU agenda. Appl Energy 2019;236:318–39. https://doi.org/10.1016/j.apenergy.2018.11.094.
[49] Instituto Nacional de Estadística (INE). Censos de Población y Viviendas 2021. https://www.ine.es/Censo2021/Inicio.do?L=0; 2025 (accessed October 9, 2023).
[50] de Santiago E, Arcas-Abella J, Pagès-Ramon A, Larrumbide E, Huerta D. Segmentación del parque residencial de viviendas en España en clústeres tipológicos. 2019.
[51] European Union. Eurostat. Energy statistics - cooling and heating degree days. https://ec.europa.eu/eurostat/cache/metadata/en/nrg_chdd_esms.htm; 2025 (accessed October 9, 2023).
[52] European Commission. JRC photovoltaic geographical information system (PVGIS) - European Commission. https://re.jrc.ec.europa.eu/pvg_tools/es/; 2025.
[53] Żukowski M. Experimental determination of the cold water temperature at the inlet to solar water storage tanks. Therm Sci Eng Progr 2020;16:1–9. https://doi.org/10.1016/J.TSEP.2019.100466.
[54] Pérez-Fargallo A, Bienvenido-Huertas D, Contreras-Espinoza S, Marín-Restrepo L. Domestic hot water consumption prediction models suited for dwellings in central-southern parts of Chile. J Build Eng 2022;49:1–13. https://doi.org/10.1016/J.JOBE.2022.104024.
[55] Gobierno de España | Ministerio de Sanidad. Capítulo 3: Sistemas de agua Caliente sanitaria [chapter 3: Domestic hot water systems]. Madrid. 2024.
[56] de la Edificación CT. Documento Básico he Ahorro de energía. CTE, DB-HE; 2022.
[57] Asociacion de Empresas El'ectricas (ASEME). DATADIS. La plataforma de datos de consumo eléctrico. https://datadis.es/; 2025 (accessed October 9, 2023).
[58] Abokersh MH, Gangwar S, Spiekman M, Vallès M, Jiménez L, Boer D. Sustainability insights on emerging solar district heating technologies to boost the nearly zero energy building concept. Renew Energy 2021;180:893–913. https://doi.org/10.1016/j.renene.2021.08.091.
[59] Tulus V, Boer D, Cabeza LF, Jiménez L, Guillén-Gosálbez G. Enhanced thermal energy supply via central solar heating plants with seasonal storage: A multi-objective optimization approach. Appl Energy 2016;181:549–61. https://doi.org/10.1016/j.apenergy.2016.08.037.
[60] De Guadalfajara M, Lozano MA, Serra LM. Evaluation of the potential of large solar heating plants in Spain. Energy Procedia 2012;30:839–48. https://doi.org/10.1016/j.egypro.2012.11.095. Elsevier Ltd.
[61] TRNSYS 18. 2023.
[62] Abokersh MH, Saikia K, Cabeza LF, Boer D, Vallès M. Flexible heat pump integration to improve sustainable transition toward 4th generation district heating. Energ Conver Manage 2020:225. https://doi.org/10.1016/j.enconman.2020.113379.
[63] Colclough S, McGrath T. Net energy analysis of a solar combi system with seasonal thermal energy store. Appl Energy 2015:147. https://doi.org/10.1016/j.apenergy.2015.02.088.
[64] Thomas LV, Schmidt O, Gambhir A, Few S, Staffell I. Comparative life cycle assessment of lithium-ion battery chemistries for residential storage. J Energy Storage 2020;28:101230. https://doi.org/10.1016/J.EST.2020.101230.
[65] Majeau-Bettez G, Hawkins TR, StrØmman AH. Life cycle environmental assessment of lithium-ion and nickel metal hydride batteries for plug-in hybrid and battery electric vehicles. Environ Sci Technol 2011;45:4548–54. https://doi.org/10.1021/es103607c.
[66] Carvalho ML, Temporelli A, Girardi P. Life cycle assessment of stationary storage systems within the italian electric network. Energies (Basel) 2021:14. https://doi.org/10.3390/en14082047.
[67] Peters JF, Baumann M, Zimmermann B, Braun J, Weil M. The environmental impact of Li-ion batteries and the role of key parameters – a review. Renew Sustain Energy Rev 2017;67:491–506. https://doi.org/10.1016/j.rser.2016.08.039.
[68] Jasper FB, Späthe J, Baumann M, Peters JF, Ruhland J, Weil M. Life cycle assessment (LCA) of a battery home storage system based on primary data. J Clean Prod 2022;366:132899. https://doi.org/10.1016/J.JCLEPRO.2022.132899.
[69] Preger Y, Barkholtz HM, Fresquez A, Campbell DL, Juba BW, Roman-Kustas J, et al. Degradation of commercial Lithium-ion cells as a function of chemistry and cycling conditions. J Electrochem Soc 2020:167. https://doi.org/10.1149/1945-7111/abae37.
[70] Saez R, Boer D, Shobo AB, Vallès M. Self-consumption potential and surplus compensation policy impact on rooftop photovoltaic systems in Spain. Renew Energy 2024:229. https://doi.org/10.1016/j.renene.2024.120713.
[71] Renewable Energy Agency I. Renewable power generation costs in 2022 2 renewable power generation costs in 2022. 2023.
[72] Giannelos S, Zhang X, Zhang T, Strbac G. Multi-objective optimization for Pareto frontier sensitivity analysis in power systems. Sustainability (Switzerland) 2024;16. https://doi.org/10.3390/su16145854.
[73] Montgomery DC. Design and analysis of experiments. John Wiley & Sons, Inc.; 2013.
[74] Global Energy Crisis. Topics - IEA. https://www.iea.org/topics/global-energy-crisis; 2025 (accessed November 18, 2024).